UNIVERSITÀ DI SIENA 1240

USiena air

Azetidin-2-one-based small molecules as dual hHDAC6/HDAC8 inhibitors: Investigation of their mechanism of action and impact of dual inhibition profile on cell viability

This is the peer reviewed version of the following article:

Original:

Federico, S., Khan, T., Fontana, A., Brogi, S., Benedetti, R., Sarno, F., et al. (2022). Azetidin-2-one-based small molecules as dual hHDAC6/HDAC8 inhibitors: Investigation of their mechanism of action and impact of dual inhibition profile on cell viability. EUROPEAN JOURNAL OF MEDICINAL CHEMISTRY, 238, 1-20 [10.1016/j.ejmech.2022.114409].

Availability:

This version is availablehttp://hdl.handle.net/11365/1208347 since 2022-09-22T09:09:41Z

Published:

DOI:10.1016/j.ejmech.2022.114409

Terms of use:

Open Access

The terms and conditions for the reuse of this version of the manuscript are specified in the publishing policy. Works made available under a Creative Commons license can be used according to the terms and conditions of said license.

For all terms of use and more information see the publisher's website.

(Article begins on next page)

19 February 2025

Azetidin-2-one-based Small Molecules as dual *h*HDAC6/HDAC8 Inhibitors: Investigation of their Mechanism of Action and Impact of Dual Inhibition Profile on Cell Viability

Stefano Federico,[a,m] Tuhina Khan,[a,m] Anna Fontana,[a] Simone Brogi,[b] Rosaria Benedetti,[c] Federica Sarno,[c] Gabriele Carullo,[a] Alex Pezzotta,[d] Akella Prasanth Saraswati,[a] Eugenia Passaro,[c] Luca Pozzetti,[a] Alessandro Papa,[a] Nicola Relitti,[e] Sandra Gemma,[a] Stefania Butini,[a] Anna Pistocchi,[d] Anna Ramunno,[f] Fabrizio Vincenzi,[g] Katia Varani,[g] Vanessa Tatangelo,[h] Laura Patrussi,[h] Cosima T. Baldari,[h] Simona Saponara,[h] Beatrice Gorelli,[h] Stefania Lamponi,[a] Massimo Valoti,[h] Fulvio Saccoccia,[i] Marialaura Giannaccari,[i] Giovina Ruberti,[i] Daniel Herp,[j] Manfred Jung,[j] Lucia Altucci,[c,k]* Giuseppe Campiani[a,]*

[a]Department of Biotechnology, Chemistry and Pharmacy, DoE Department of Excellence 2018-2022, University of Siena, 53100 Siena, Italy;

[b]Department of Pharmacy, University of Pisa, 56126 Pisa, Italy;

[c]Department of Precision Medicine, University of Campania Luigi Vanvitelli, 80138 Naples, Italy;

[d]Department of Medical Biotechnology and Translational Medicine, University of Milan, LITA - Via Fratelli Cervi 93, 20090 Segrate (MI) Italy;

[e]IRBM Science Park, Via Pontina km 30,600, 00071 Pomezia, Rome, Italy;

[f]Department of Pharmacy, University of Salerno, 84084 Fisciano (SA), Italy;

[g]Department of Translational Medicine, University of Ferrara, 44121 Ferrara, Italy;

[h]Department of Life Sciences, University of Siena, 53100 Siena, Italy;

[i]Institute of Biochemistry and Cell Biology (IBBC), National Research Council (CNR), 00015 Monterotondo (Rome), Italy;

[j]Institute of Pharmaceutical Sciences, Albert-Ludwigs-Universität Freiburg, 79104 Freiburg, Germany;

[k]BIOGEM, Molecular Biology and Genetics Research Institute, Ariano Irpino (AV), Italy

[m]these authors are joint co-first authors

Authors for correspondence: campiani@unisi.it (G.C.), lucia.altucci@unicampania.it (L.A.)

ABSTRACT

The search of new therapeutic tools for the treatment of cancer is being a challenge for medicinal chemists. Due to their role in different pathological conditions, histone deacetylase (HDAC) enzymes are considered valuable therapeutic targets. HDAC6 is a well-investigated HDAC-class IIb enzyme mainly characterized by a cytoplasmic localization; HDAC8 is an epigenetic eraser, unique HDAC-class I member that displays some aminoacidic similarity to HDAC6. New polypharmacological agents for cancer treatment, based on a dual *h*HDAC6/*h*HDAC8 inhibition profile were developed. The dual inhibitor design investigated the diphenyl-azetidin-2-one scaffold, typified in three different structural families, that, combined to a slender benzyl linker (**6c**, **6i**, and **6j**), displays nanomolar inhibition potency against both isoforms, *h*HDAC6 and *h*HDAC8. Notably, their selective action was also corroborated by measuring their low inhibitory potency towards *h*HDAC1 and *h*HDAC10. Selectivity of these compounds was further demonstrated in human cell-based western blots experiments, by testing the acetylation of the non-histone substrates alpha-tubulin and SMC3. Furthermore, the compounds reduced the proliferation of colorectal HCT116 and leukemia U937 cells, when tested for 48 hours of treatment. The toxicity of the compounds has been evaluated in rat perfused heart and in zebrafish embryos. In this latter model we also validated the efficacy of the dual *h*HDAC6/*h*HDAC8 inhibitors against their common target acetylated-alpha tubulin. Finally, the metabolic stability has been verified in rat, mouse, and human liver microsomes.

Keywords

HDAC6; HDAC8; azetidin-2-one; colorectal cancer; leukemia; HDAC inhibitors.

Abbreviations

AcOH: acetic acid; ARID1a: AT-rich interactive domain-containing protein 1A; CDI: 1,1'-carbonyldiimidazole; Cl_{int}: intrinsic clearance; DCM: dichloromethane; DIPEA: *N,N*-Diisopropylethylamine; DMF: *N,N*-dimethylformamide; DMSO: dimethyl sulfoxide; dpf: days post-fertilization; ECG: electrocardiogram; EDCI: 1-ethyl-3-(3-dimethylaminopropyl)carbodiimide; ERRα: estrogen-related receptor alpha; H_2: molecular hydrogen; H_2O: water; H3K9-14: histone H3 lysines 9 and 14; HDAC: histone deacetylase; HLM: human liver microsomal preparations; HOBt: 1-Hydroxybenzotriazole; HR: frequency; HSP90: heat shock protein 90; *k*: apparent decay constant; KOH: potassium hydroxide; LiOH: lithium hydroxide, MeI: methyl iodide; MeOH: methanol; MLM: mouse liver microsomal preparations; MTT: 3-(4,5-dimethylthiazol-2-yl)-2,5-diphenyltetrazolium bromide; $NaBH_3CN$: sodium cyanoborohydride; $NaBH_4$: sodium borohydride; NaOH: sodium hydroxide; NH_2OH: hydroxylamine; $NiCl_2{\cdot}6H_2O$: nickel(II) chloride hexahydrate; p53: cellular tumor antigen p53; PARP: poly (ADP-ribose) polymerase; PCI: PCI34051; PDB: protein data bank; Pd-C: palladium on activated carbon; PQ: atrioventricular conduction time; pSTAT3: phosphorylated form of signal transducer and activator of transcription 3; PTM: post-translational modifications; QRS: intraventricular conduction time; QT: duration of ventricular depolarization and repolarization, i.e., the action potential duration; QTc, corrected QT; RLM: rat liver microsomal preparations; RR: cycle length; SAHA: suberoylanilide hydroxamic acid or vorinostat; SAR: structure-activity relationship; SD: standard deviation; SI: selectivity index; SMC3: structural maintenance of chromosomes protein 3; $t_{1/2}$: half-life time; TEA: triethylamine; TEBAC: benzyltriethylammonium chloride; TFA: trifluoroacetic acid; THF: tetrahydrofuran; TLC: thin-layer chromatography; TPSA: topological polar surface area; TUB: tubastatin A; UV: ultraviolet; ZBG: zinc binding group.

1. Introduction

For many years, cancer has been considered as the result of DNA mutations prompting the activation of oncogenes or the inactivation of tumor suppressor genes [1]. However, it was proved that epigenetic modifications can alter gene expression, thus playing a crucial role in the regulation of the neoplastic processes [2]. These structural modifications (or post-translational modifications (PTM)) of chromatin determine a change in the accessibility of the DNA therefore regulating gene expression [3]. Three specific classes of enzymes are responsible for PTM of histones: writers, erasers, and readers. Among the eraser enzymes, histone deacetylases (HDACs) deacetylate histones and non-histone proteins involved in cell signaling, apoptosis, DNA transcription, repair, and replication. To date, 18 HDAC isoforms have been identified and divided into four classes. HDAC6 is a class IIb enzyme possessing a distinctive structure and mostly localized in the cytoplasm. HDAC6 has a catalytic activity against mainly non-histone substrates, the most relevant of which are α-tubulin, heat-shock protein 90 (Hsp90), cortactin, peroxiredoxin, and tau proteins [4]. The dysregulated activity of HDAC6 has been associated with the pathogenesis of several diseases including cancer and rare disorders [4–7]. HDAC8 belongs to class I enzyme and shows both nuclear and cytosolic localization. HDAC8 differs in aminoacidic sequence from the other class I HDACs (1-3)[8,9], it is smaller in size and acts independently as it lacks the C-terminal protein-protein interaction domains that favor the incorporation into multiprotein complexes. SMC3, p53, ERRα, and ARID1a are the most relevant substrates of HDAC8 [10]. HDAC8 is implicated in various cellular processes (e.g., sister chromatid separation, energy homeostasis, microtubule integrity, and muscle contraction) therefore it could be a valuable therapeutic target in several diseases including cancer, X-linked intellectual disability and parasitic infections [11,12]. The crucial role of HDACs activity in tumorigenesis has been investigated; many lymphoid malignancies showed an overexpression or overactivity of HDACs. Of note, the reduced HDAC-mediated acetylation has been directly correlated with the proliferation and survival of lymphoma cells [3]. In this context, the efficacy of pan-HDAC inhibitors (HDACis) has been widely demonstrated thus leading to the approval of some

drugs such as vorinostat [13] and romidepsin [14] for the treatment of different hematological malignancies. Furthermore, also ricolinostat (**1**, Figure 1) is currently under study for the treatment of cutaneous T-cell lymphoma. On the other hand, belinostat (**2**, Figure 1) [15] and tucidinostat (**3**, Figure 1) [16] are investigated for relapsed or refractory peripheral T-cell lymphoma, and panobinostat for multiple myeloma [17]. However, due to their non-selective profile (they act also as HDAC1 inhibitors), their action is characterized by several drawbacks [18,19]. From a biochemical point of view, selective HDAC6 inhibition, induced by quinolone derivative **4** (Figure 1), stimulates apoptosis in colorectal cancer cells through PARP cleavage *via* a pSTAT3-dependent activity [20,21]. Other studies showed how well known HDAC6 inhibitors such tubastatin A (TUB) and **1** failed to show significant anti-cancer properties [22]. HDAC8 deregulation has been correlated with the development of leukemia, neuroblastoma, as well as colorectal cancer. Blood cancer cells, treated with the selective HDAC8 inhibitor PCI-34051 (PCI, **5**, Figure 1), undergo apoptosis through a calcium/caspase-dependent mechanism [11,23]. Other studies in colorectal cancer cells showed that HDAC8 inhibition is related to pSTAT3-dependent apoptosis and to the transcription of specific genes as *BMF* and *LHx1* [24,25]. Most of the HDACis developed to date share a common pharmacophoric structure, which encompasses three main portions: a zinc-binding group (ZBG), a surface recognition group (cap), and a linker moiety connecting them. Our research group has been actively involved in the synthesis of selective *h*HDAC6is and *Schistosoma mansoni (Sm)*HDAC8is as potential therapeutic tools for the treatment of rare disorders such Rett syndrome [5], idiopathic pulmonary fibrosis [7], retinitis pigmentosa [26], cancer [20,21], and schistosomiasis [12]. The design of inhibitors endowed with a dual *h*HDAC6/*h*HDAC8 profile (but selective with respect to *h*HDAC1) remains highly challenging. Taking inspiration from *h*HDAC6/*h*HDAC8 similarities in the active site [9], and given that they share key substrate proteins, such as α-tubulin [27], we performed extensive research to rationally identify dual-acting small molecules. Up to date, few compounds have been reported as selective *h*HDAC8 inhibitors and a lesser number are truly selective for both *h*HDAC6 and *h*HDAC8 over other class I and class IIb HDAC isoforms [28,29]. Very recently, a family of di-

hydroxamic acid derivatives has been reported to inhibit HDACs, including HDAC8, promoting SMC3 and tubulin acetylation [30]. Targeting almost two HDAC isoforms is a valuable strategy for the development of new drugs with synergistic efficacy combined to minimal side effects. In addition, HDAC6 and HDAC8 simultaneous inhibition could potentially abrogate any functional redundancy exhibited by these enzymes [31]. In particular, inhibition of HDAC8 has shown promise as an effective strategy for treating various cancers, while inhibition of HDAC6 is useful also due to its effects on the ubiquitin pathway as a single agent and in combination therapies [32]. Dual inhibition of these two isoforms could provide a larger therapeutic window and have beneficial additive or synergistic effects in neoplastic disorders [28]. In this context, we investigated a combination of bulky cap groups and specific slender linkers to identify new molecular hits that suitably fit into both *h*HDAC6 and *h*HDAC8 catalytic sites. We identified the diphenylazetidin-2-one as a privileged scaffold and innovative cap-group to develop a new generation of dual-acting *h*HDAC6/8 inhibitors. Strategically, we developed a library of azetidin-2-ones to be explored for their inhibitory activity towards *h*HDAC6 and *h*HDAC8 over nuclear class I *h*HDAC1 and class IIb *h*HDAC10 isoforms. The best performing compounds **6c**, **6i**, and **6j** were evaluated as antiproliferative agents in leukemia U937 (overexpressing HDAC6, Figure S1) [33] and colorectal HCT116 (overexpressing HDAC8, Figure S1) [34] cell lines, as models of hematological and solid malignancies, respectively [11]. Additionally, we evaluated their toxicity in vitro against NIH3T3 cells and *in vivo* using the zebrafish (*Danio rerio*) model. Their metabolic profile was determined in rat, mouse, and human liver microsomes while other physicochemical properties were calculated in silico. Finally, the cardiotoxic potential was assessed for **6j**, representative hit candidate of this novel class of dual *h*HDAC6/8 inhibitors.

2. Results and Discussion

2.1 Chemistry

The chemical structures of compounds **6a-m** are reported in Table 1. In order to get a deeper understanding of the azetidin-2-one core as cap group in terms of selectivity and inhibitory potency towards the different HDACs isoforms, three sets of compounds were developed. The first set is characterized by the presence of two phenyl rings at positions C3 and C4 of the azetidin-2-one core in the *trans* configuration, the second one bears both phenyl substituents on the C3 position, while the third set displays the presence of a single phenyl group at C4 position.

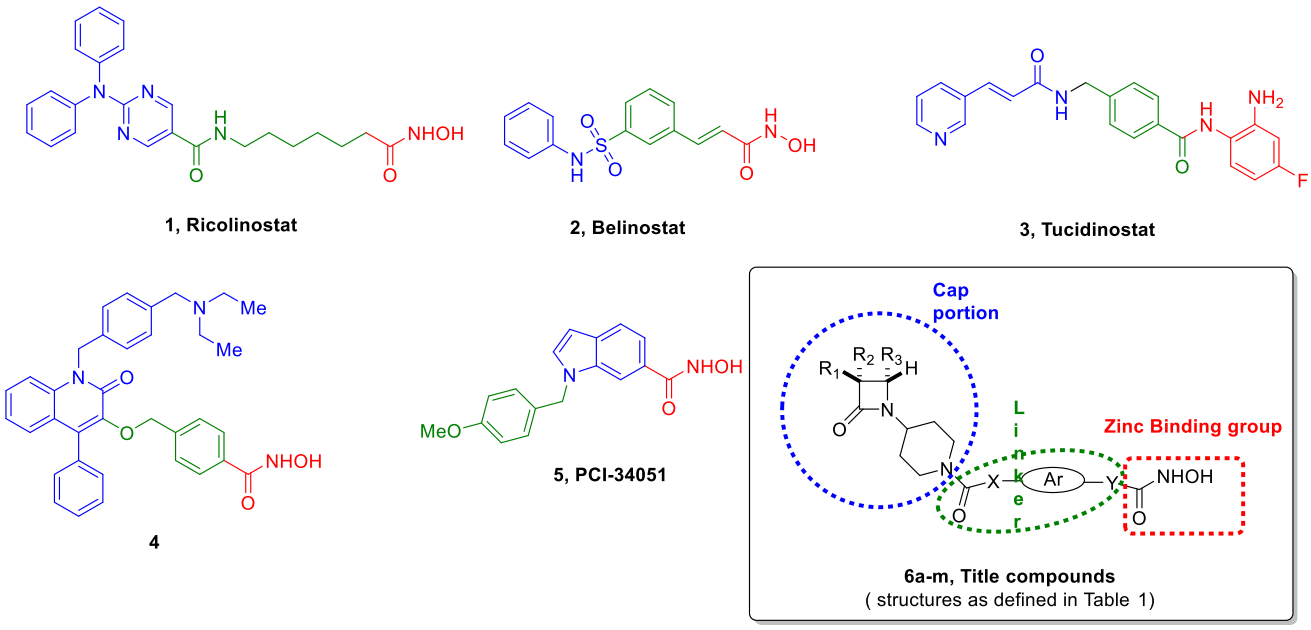

Figure 1. Representative HDACis approved for therapy (**1-3**); a selective *h*HDAC6 inhibitor (**4**); a selective HDAC8 inhibitor (**5**) and newly designed azetidin-2-one-based HDAC inhibitors **6a-m**

As described in Scheme 1, the vicinal azetidin-2-one derivatives **(±)-6a-h** were synthesized starting from the azetidin-2-one-based intermediate **(±)-8**, obtained from the previously described compound **7**. The latter reaction gave the β-lactam-based compound in *trans* configuration as previously described by us [35,36]. In particular, the coupling constant of proton H3 and H4 in azetidin-2-one ring are indicative of the proposed stereochemistry with a J_{H_3,H_4} = 2.2 Hz (J_{H_3,H_4} > 4.0 Hz for the *cis* stereoisomer; $J_{H_3,H_4} \leq 3.0$ Hz for the trans stereoisomer, see experimental section) as also previously reported [37,38]. Removal of the benzyl group on the piperidine moiety of **(±)-8** by

catalytic hydrogenation furnished the free amine **(±)-9**. The latter was then reacted with appropriate isocyanates or carboxylic acids, prepared according to literature procedures [20,39–44], in order to obtain ureas **(±)-10a**, **(±)-10c**, **(±)-10h**, and amides **(±)-10b**, **(±)-10d-g**, respectively. Intermediates **(±)-10a-h** were then converted into the corresponding hydroxamic acids **(±)-6a-h** after treatment with NH_2OH and a methanolic solution of KOH.

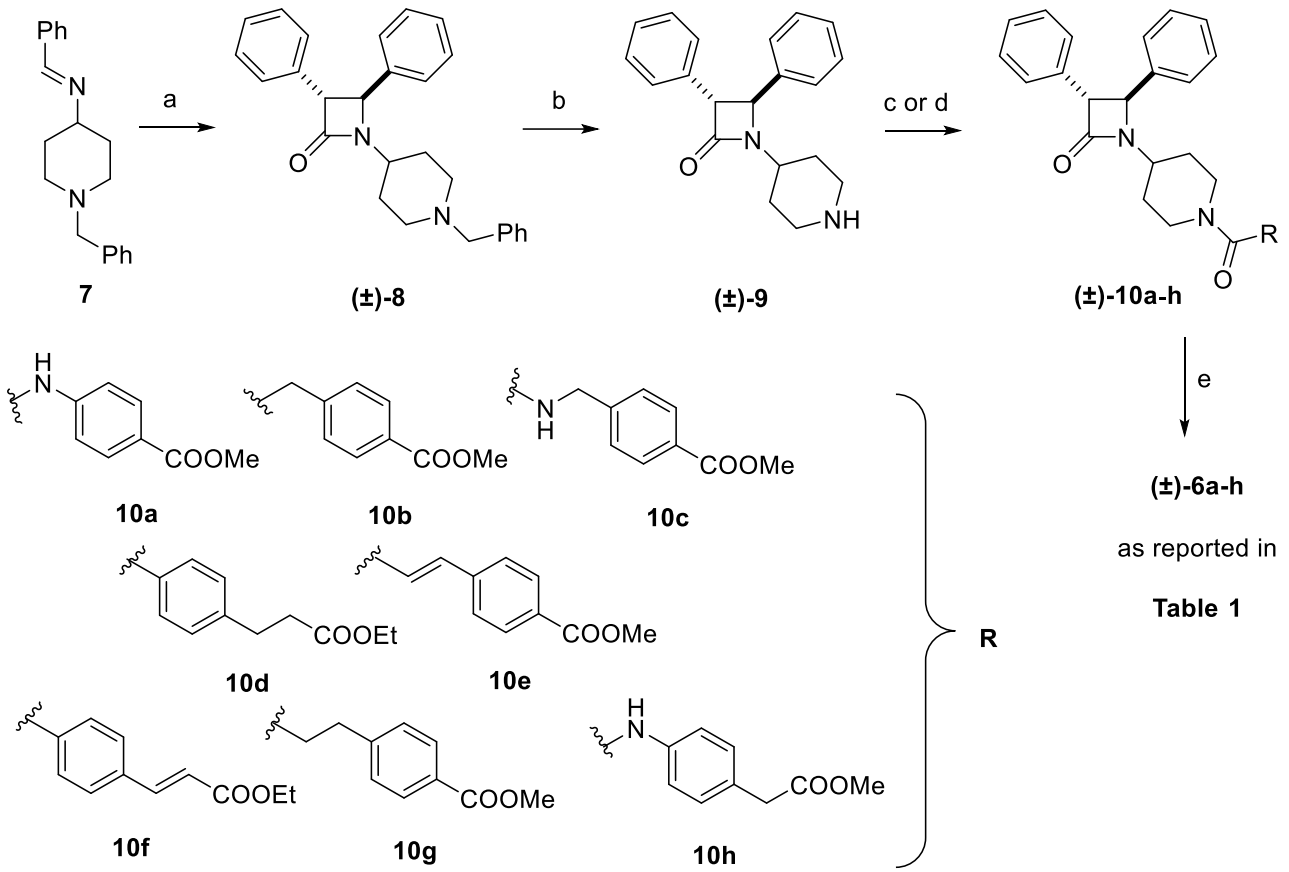

Scheme 1. Synthesis of vicinal derivatives **(±)-6a-h.** a) phenylacetic acid, triphosgene, dry DCM, 50 °C, 12 h; then **7**, TEA, 50 °C, 12 h; b) Pd-C, H_2, MeOH, 25 °C, 12 h; c) appropriate isocyanate, TEA, dry THF, 65 °C, 1.5 h (for **10a**, **10c**, and **10h**); d) appropriate carboxylic acid, DIPEA, EDCI, HOBt, dry DCM, 0 °C to 25 °C, 12 h (for **10b** and **10d-g**); e) NH_2OH (50 wt. % in H_2O), 4 N KOH in MeOH, DCM/MeOH (1:2), 25 °C, 2 h.

In Scheme 2 the synthesis of the second class of HDACis is reported. Starting from commercially available 4-amino-1-benzylpiperidine **11**, dimethyl dithioiminocarbonate (**12**) was obtained after treatment with carbon disulfide and methyl iodide [45]. As previously described by us, this intermediate, replacing the canonical imine, was submitted to a non-photochemical [2+2]

cycloaddition with diphenylacetic acid and triphosgene to yield the achiral azetidin-2-one core **13** [46]. The reduction of the *bis*(thiomethyl) group of **13** was achieved with sodium borohydride in the presence of nickel chloride hexahydrate to produce the geminal *bis*(phenyl) derivative **14** which, after catalytic hydrogenation, yielded the key intermediate **15**. As for Scheme 1, amine **15** was reacted with the appropriate acid, isocyanate, or alcohol to obtain amide **16a**, urea **16b**, and the carbamate **16c**, according to literature procedures [20,47]. Finally, intermediates **16a-c** were converted into the corresponding hydroxamic acids **6i-k** as already described in Scheme 1.

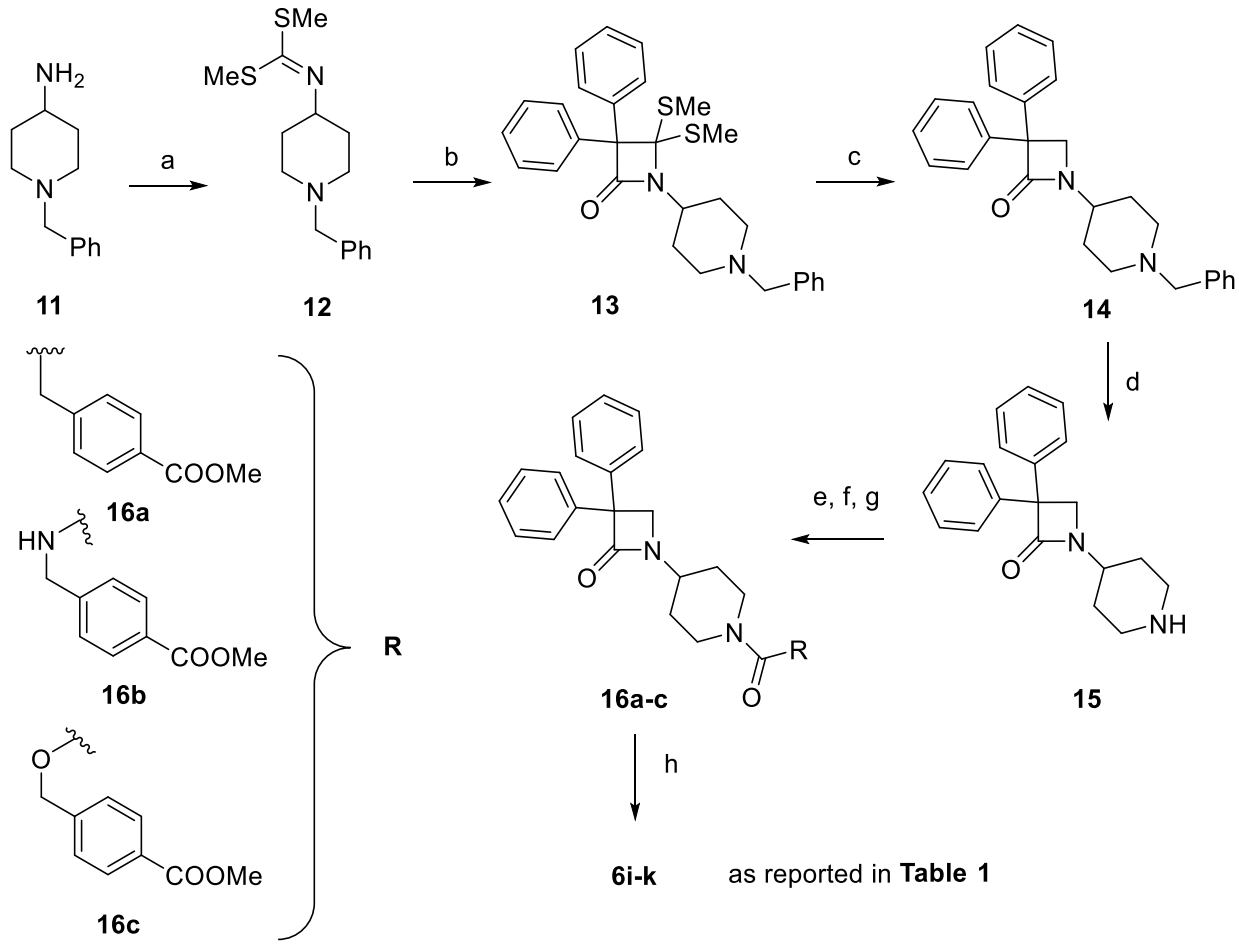

Scheme 2. Synthesis of geminal derivatives **6i-k**. a) CS_2, 20 N NaOH in H_2O, toluene, 0 °C, 5 min; then MeI, TEBAC, toluene, 25 °C, 30 min; b) diphenylacetic acid, triphosgene, TEA, dry DCM, 50 °C, 12 h; c) $NaBH_4$, $NiCl_2 \cdot 6H_2O$, MeOH, THF, 25 °C, 12 h; d) Pd-C, H_2, MeOH, 25 °C, 12 h; e) 2-(4-(methoxycarbonyl)phenyl)acetic acid, DIPEA, EDCI, HOBt, dry DCM, 0 °C to 25 °C, 12 h (for **16a**); f) methyl 4-(isocyanatomethyl)benzoate, TEA, dry THF, 65 °C, 1.5 h (for **16b**); g) methyl 4-(hydroxymethyl)benzoate, CDI, DCM, 0 °C to 25 °C, 6 h (for **16c**); h) NH_2OH (50 wt. % in H_2O), 4 N KOH in MeOH, DCM/MeOH (1:2), 25 °C, 2 h.

The third class of azetidin-2-one compounds was synthesized according to **Scheme 3**. The amino acid methyl esters **17a**,**b**, obtained as previously described [48,49], underwent reductive amination with *N*-Boc-piperidone affording intermediates **(±)-18a**,**b**, which were then subjected to basic hydrolysis of the ester group followed by an intramolecular cyclization in presence of Mukaiyama's salt, thus affording azetidin-2-one derivatives **(±)-19a**,**b**. These intermediates were deprotected under acidic conditions, affording amines **(±)-20a**,**b**, followed by reaction with methyl 4-(isocyanatomethyl)benzoate to obtain ureas **(±)-21a**,**b**, which were finally converted into the corresponding hydroxamates **(±)-6l** and **(±)-6m**.

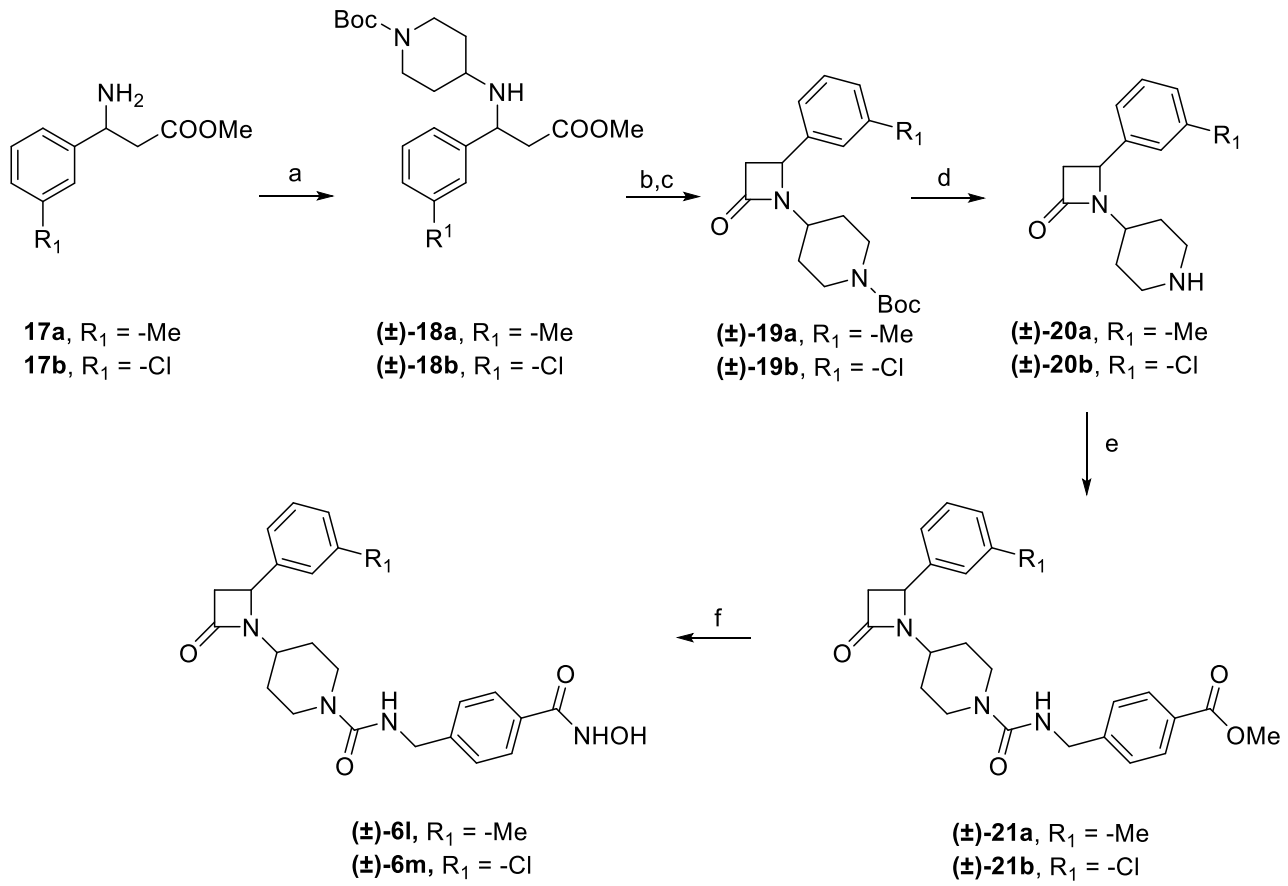

Scheme 3. Synthesis of C4-substituted derivatives **6l**,**m**. a) *N*-Boc-piperidone, DIPEA, AcOH, DMF, 25 °C, 12 h, then $NaBH_3CN$, 25 °C, 12 h; b) LiOH, THF/MeOH/H_2O (1:1:1), 25 °C, 12 h; c) 2-chloro-1-methylpyridinium iodide, TEA, MeCN, 80 °C, 12 h; d) TFA, DCM, 0 °C to 25 °C, 1 h; e) methyl 4-(isocyanatomethyl)benzoate, TEA, 65 °C, 2 h; f) NH_2OH (50 wt. % in H_2O), 4 N KOH (in MeOH), DCM/MeOH (1:2), 25 °C, 2 h.

Table 1. Inhibitory activity of compounds **6a-m** toward *h*HDAC1 (as IC_{50}, µM) and *h*HDAC6 (as IC_{50}, nM). Inhibition activity towards *h*HDAC8 (as IC_{50}, nM) and *h*HDAC10 (as IC_{50}, µM) for selected compounds.

Compound	Structure	IC_{50} *h*HDAC1 (nM)	IC_{50} *h*HDAC6 (nM)	IC_{50} *h*HDAC8 (nM)	IC_{50} *h*HDAC10 (nM)	SI (HDAC6/8)	SI (HDAC1/6)	SI (HDAC1/8)
(±)-6a	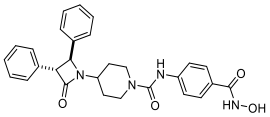	1270 ± 100	203.3 ± 10.4	NT	NT			
(±)-6b	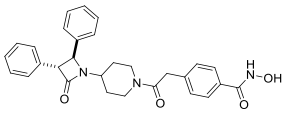	5140 ± 710	121 ± 8	NT	NT			
(±)-6c	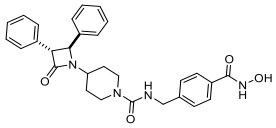	4200 ± 200	21 ± 1	42 ± 4	6600 ± 400	2	200	100
(±)-6d	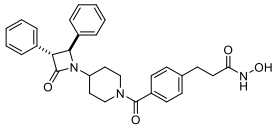	@50 µM: 89.5% @10 µM: 66.4% @1 µM: 22.3%	@50 µM: 98.4% @10 µM: 85.7% @1 µM: 35.9%	NT	NT			
(±)-6e	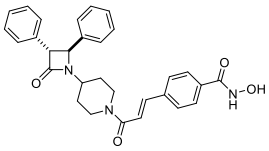	@50 µM: 100,1% @10 µM: 90.1% @1 µM: 49.7%	130.0 ± 24.1	NT	NT			
(±)-6f	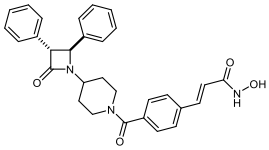	@50 µM: 97.3% @10 µM: 93.4% @1 µM: 61.0%	168.4 ± 25.1	NT	NT			
(±)-6g	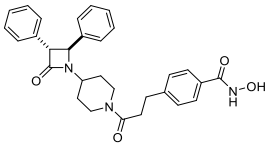	@50 µM: 83.6% @10 µM: 48.7% @1 µM: 17.2%	@50 µM: 102.4% @10 µM: 97.1% @1 µM: 69.7%	NT	NT			
(±)-6h	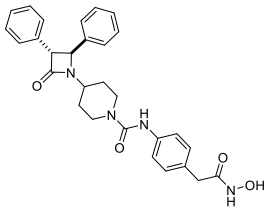	@50 µM: 82.7% @10 µM: 53.3% @1 µM: 23.6%	@50 µM: 102.6% @10 µM: 94.2% @1 µM: 60.2%	NT	NT			

6i	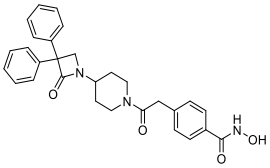	9700 ± 390	91 ± 7	113 ± 2.6	5100 ± 300	1	106	86
6j	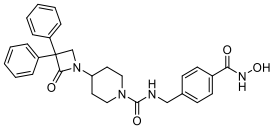	4300 ± 300	3.4 ± 0.8	99 ± 2.1	6500 ± 400	29	1264	43
6k	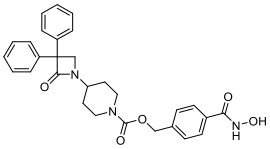	4100 ± 100	18.5 ± 1.2	@50μM: 13%	NT			
(±)-6l	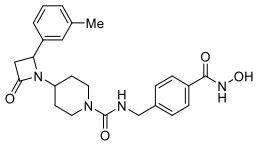	3100 ± 200	399 ± 5.5	NT	NT			
(±)-6m	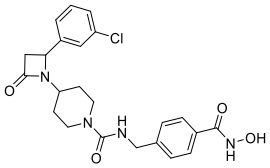	15100 ± 600	270 ± 22	NT	NT			

Each value is the mean of at least three determinations; results are expressed with ±standard deviation (SD). When not specified, SD is <10% of the IC_{50}. NT: not tested.

2.2. Docking studies of **6c** *into the hHDAC1, hHDAC6 and hHDAC8 catalytic sites and SARs of* **6a-m**

To investigate SARs of this novel class of compounds, **6a-m** were tested for their ability to inhibit *h*HDAC6 and *h*HDAC1. Selected compounds **6c**, **6i**, and **6j** were tested against *h*HDAC8 and *h*HDAC10 in order to determine the selectivity profile in terms of isoforms of interest. The selection strategy of bulkier cap group for improving the selectivity towards HDAC6 and HDAC8 over HDAC1 is reported in the Supplementary Materials (Figure S1). To gain insights into the possible mechanism governing the inhibitory activity of these compounds, we performed molecular docking calculations employing compound **6c** as the prototypic compound of the series, being experimentally characterized as one of the most potent dual-inhibitor of *h*HDAC6/8. The computational studies were

performed by applying a docking protocol as described by us [20,21,50], the output for which is illustrated in Figure 2.

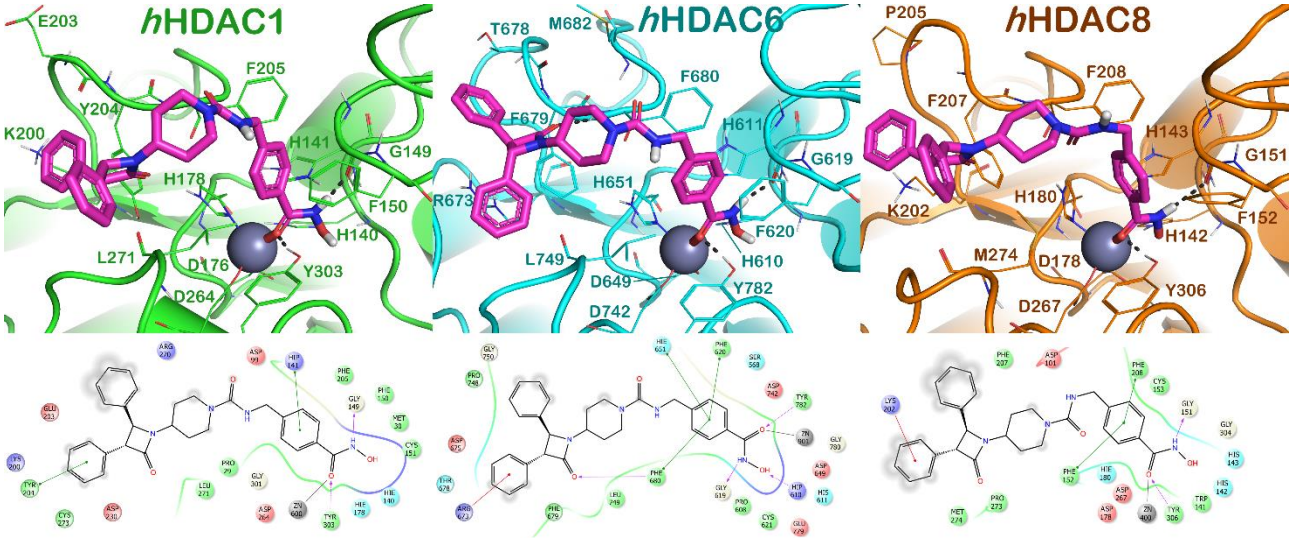

Figure 2. Putative binding modes of **6c** (magenta sticks) into *h*HDAC1 (PDB ID 4BKX, green cartoon) *h*HDAC6 (PDB ID 5EDU, cyan cartoon) *h*HDAC8 (PDB ID 3F0R, orange cartoon). Residues in the active sites are represented by lines and the Zn^{2+} is represented by a gray sphere. H-bonds are represented by black dotted lines. Pictures were generated by means of PyMOL, while ligand-interaction diagram were generated by Maestro.

In particular, we observed an increase in relevant contacts when the compound interacted with *h*HDAC6 and *h*HDAC8 binding sites, with respect to the interactions produced within *h*HDAC1 binding site. In fact, **6c** established a limited number of polar and non-polar contacts within *h*HDAC1 with its hydroxamic moiety, two H-bonds with G149 and Y303, in addition to the metal coordination bond. The benzyl linker was able to form a π-π stacking with H141, while one aromatic ring belonging to the β-lactam moiety was involved in a π-π stacking with Y204. Considering the model of interaction obtained for the complex **6c**/*h*HDAC6, we observed a dramatic increase in the number of contacts established by **6c** within the *h*HDAC6 binding site. In this case, the hydroxamic moiety, in addition to the metal coordination bond, established two H-bonds with G619 and Y782, while the benzyl linker interacted with H651, F620, and F680 by three π-π stacking. The β-lactam moiety

formed a H-bond with the backbone of F680 by the carbonyl belonging to the β-lactam ring, while the benzyl substituent interacted with R673 by a cation-π stacking. Finally, considering the complex **6c**/*h*HDAC8, we observed a slight decrease in the number of contacts with respect to those found by analyzing **6c**/*h*HDAC6 complex. In fact, the hydroxamic moiety of **6c**, in addition to the metal coordination bond, established two H-bonds with G151 and Y306, the benzyl linker interacted with F152 and F208 by two π-π stacking, while the phenyl substituent present on the β-lactam moiety formed a cation-π stacking with K202. The differences found for **6c** in interacting with the three selected *h*HDAC binding sites accounted for different docking scores (**6c**/*h*HDAC1 = -6.738 kcal/mol; **6c**/*h*HDAC6 = -9.357 kcal/mol; **6c**/*h*HDAC8 = -8.576 kcal/mol) that supports the different inhibitory potency found in the enzymatic tests (**6c**, IC_{50} *h*HDAC1 = 4.2 µM; IC_{50} *h*HDAC6 = 21 nM; IC_{50} *h*HDAC8 = 42 nM).

Once investigated the mode of action of our prototypic compound we investigated the SARs of the series. Compound **6a** showed an IC_{50} value of 203 nM against *h*HDAC6, with very low selectivity over *h*HDAC1, probably due to the short linker chain (according with literature data, a cut-off for selectivity index is (SI) > 30 [51]). When the urea bridge was replaced with a benzyl amide, as in compound **6b**, the *h*HDAC6 inhibitory potency increases with IC_{50} value equal to 121 nM, with a slightly better selectivity over *h*HDAC1 (SI 43). The homologation n of the aryl urea system (from aryl urea to a benzyl urea) as in **6c** led to a significant improvement in *h*HDAC6 inhibitory potency (IC_{50} value of 21 nM) and to an interesting increase in the selectivity over *h*HDAC1. Analogue **6c**, prototypic of the *trans*-3,4-diphenylazetidin-2-one series of inhibitors, was the most potent *h*HDAC6i. Furthermore, transformation of **6b** into the vinylogous cinnamic amide (**6e**) and cinnamic hydroxamic acids (**6f**) maintained potency against *h*HDAC6 while reduced affinity for *h*HDAC1. Moreover, homologation of **6b** into **6g** reduced inhibitory activity against *h*HDAC6 and *h*HDAC1. Replacement of the benzhydroxamic acid moiety of **6b** by an *N*-hydroxyphenylpropionamide system (**6d**) or introduction of the benzylhydroxamate as in **6h** led to almost inactive analogues. Further computational studies prompted us to convert the *trans*-3,4-diphenylazetidin-2-one cap group into a

geminal 3,3-diphenyl-substituted one, characterized by the lack of the chiral centers. Maintaining the benzylic linker moiety of the best performing compounds **6b**,**c**, the synthesized compound **6i**, analogous to **6b**, showed potency in the same range of activity, while the analogue of **6c**, namely **6j**, showed an enhanced IC_{50} value equal to 3.4 nM, with a better SI of 1264 over *h*HDAC1. **6j** was identified as one of the most potent *h*HDAC6 inhibitor with a great selectivity profile over *h*HDAC1. The switch of urea into a carbamate led to compound **6k**, which maintained the high potency *vs* *h*HDAC6 in the nanomolar range. In fact, the carbamate functional group coupled to a geminal 3,3-diphenyl-substituted betalactam (**6k**), did not allow a correct accommodation within the *h*HDAC8 binding site, lacking most of the interactions described for compound **6c**. The output of docking calculation is reported in Figure S2. To further explore the SAR, we also approached the synthesis of 4-monosubstituted azetidin-2-one derivatives. The newly developed ureas **6l** and **6m** showed a decreased potency against *h*HDAC6, even if dependent upon the nature of the substituent in the pendant phenyl ring. Since one of the objectives of the present research effort was to combine *h*HDAC6 inhibition to that for *h*HDAC8 we initially investigated **6c** and **6j** using an *h*HDAC8 homology model. Virtual screening highlighted an interesting pattern of interaction which was confirmed in *h*HDAC8 inhibitory assays. *In vitro* assays on the most active and selective *h*HDAC6 inhibitors showed how **6c**, **6i** and **6j** were able to inhibit *h*HDAC8 with very low IC_{50} values (42-113 nM), thus validating these compounds as new poly-pharmacological tools. To further confirm the dual *h*HDAC6/*h*HDAC8 selectivity, due to the specific structural features of the molecules, we performed *in vitro* inhibition assays using *h*HDAC10, which together with *h*HDAC6 belongs to the class IIb of enzymes [9]. All tested compounds showed IC_{50} values >5000 nM, thus confirming their selective inhibition profile towards *h*HDAC6/*h*HDAC8 over *h*HDAC1 and *h*HDAC10.

2.3. HDACs inhibitory profile: western blot analysis in cellular models

To determine whether selected compounds **6c**, **6i** and **6j**, displayed preferential inhibitory activity among HDACs, the acetylation levels of tubulin, HSP90, H3K9-14 and SMC3 were firstly analyzed

in comparison with the pan-HDAC inhibitor SAHA. As shown in Figure 3, western blot analysis supported **6c**, **6i**, and **6j** HDAC inhibitory activity in both U937 and HCT116 cells. At 24 and 48 h, using SAHA (10 μM) as the reference compound, **6c**, **6i**, and **6j** (10 μM) were able to increase the acetylation levels of tubulin (Figure 3, panels A and B), HSP90 (Figure 3, panels C and D) and H3K9-14 (Figure 3, panels E and F). Although **6c**, **6i**, and **6j** induced a slight increase in histone acetylation, the increase in tubulin acetylation is so dramatic to suggest the binding preferentiality for HDAC6. To confirm this behavior, we evaluated also the acetylation levels of α-tubulin comparing the effect with the known HDAC6 inhibitor TUB (10 μM). As reported in Figure 4, the levels of acetylated α-tubulin are comparable among the compounds and TUB, with high levels for the compounds in U937 cells. HDAC8 inhibition was instead assessed through the increase of acetyl SMC3 (Lys105/106) (Figure 4). PCI (10 μM), a potent and selective HDAC8 inhibitor, was used as a positive control [52]. SMC3 is a subunit of cohesin, a protein complex involved in chromosome organization [53,54], that is acetylated during S-phase and deacetylated in anaphase by HDAC8 [55]. In U937 cells, **6c**, **6i**, and **6j** induced an increase in SMC3 acetylation levels at 48 h of treatment, despite a lower level than PCI (Figure 4A). Also in HCT116 cells **6c**, **6i**, and **6j** showed enhanced acetyl SMC3 levels, although the effect is more evident after 24 hours of treatment (Figure 4B). In both cell lines however, **6j** showed the strongest increase in AcetylSMC3 level. The different timing for U937 and HCT116 cell lines should be partially explained by the ratio between HDAC6 and HDAC8 expression in both systems (Figure S3).

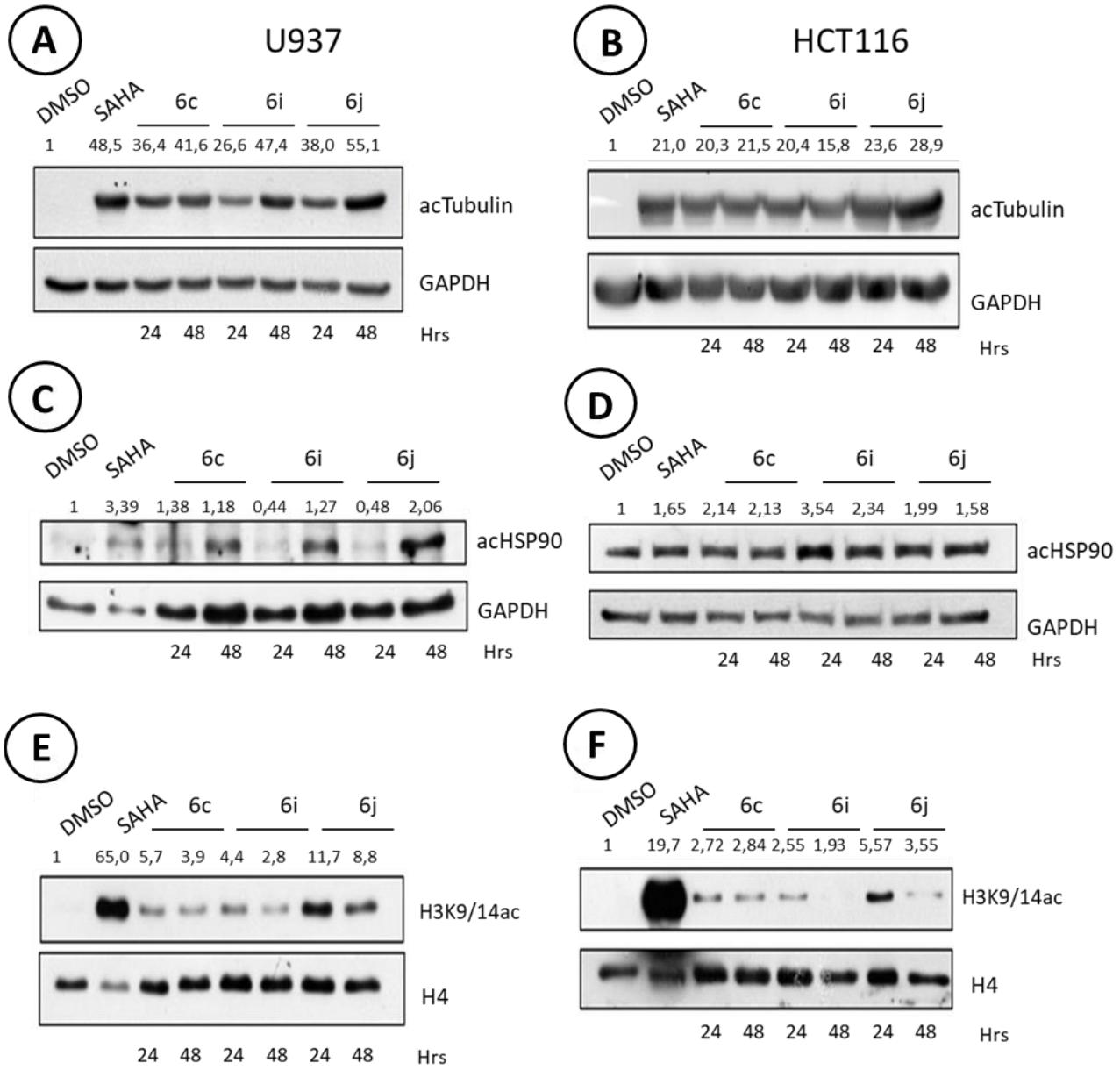

Figure 3. Western blot analyses of α-tubulin (panels **A**, **B**), HSP90 (panels **C**, **D**), and H3K9-14ac (panels **E**, **F**) acetylation after 24 and 48 h treatment of U937 (left) and HCT116 (right) cells with compounds **6c**, **6i**, and **6j** at 10 μM concentration. SAHA was used as the positive control. Semi-quantitative analysis was performed using ImageJ software and the relative intensities are reported in numbers.

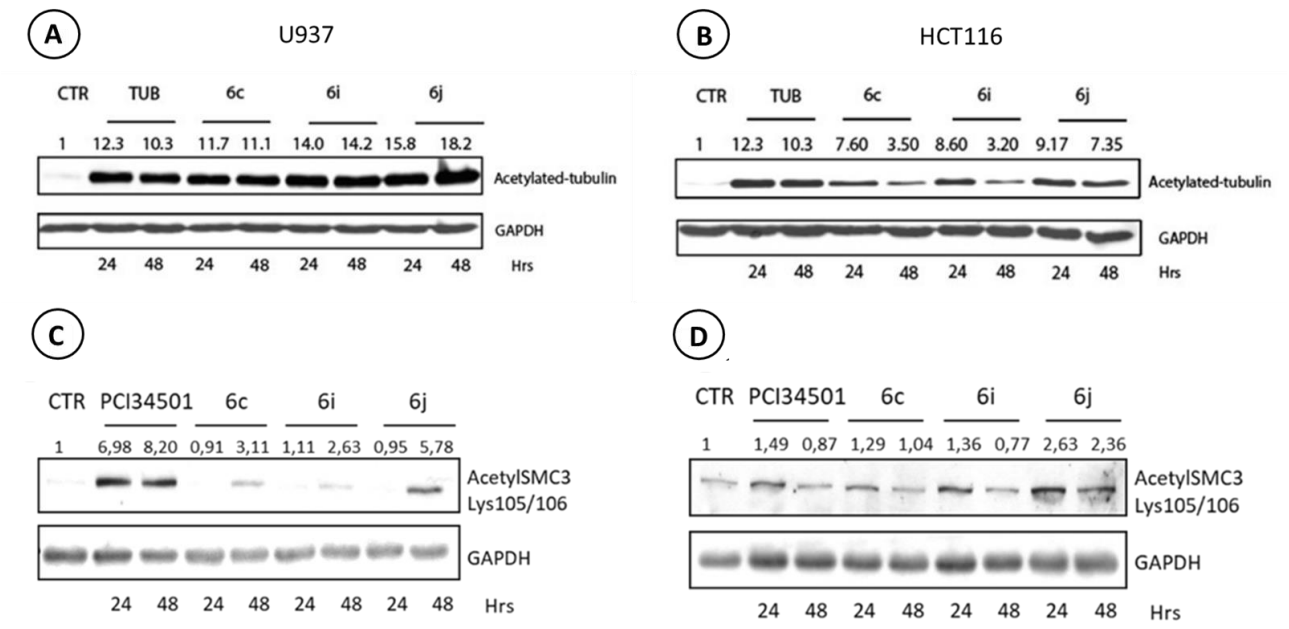

Figure 4. Western blot analyses of alpha-tubulin acetylated of U937 (Panel A) and HCT 116 cells (Panel B) treated with TuB and compounds **6c**, **6i** and **6j**. SMC3 acetylation of U937 (Panel C) and HCT116 (Panel D) cells with **6c**, **6i**, and **6j** compounds after 24-48 h of treatment at 10 µM concentration. PCI was used as the positive control. Semi-quantitative analysis was performed using ImageJ software and the relative intensities are reported in figures.

2.4. Evaluation of the anti-proliferative activity in U937 and HCT-116 cell lines

The effect on cell viability of **6c**, **6i**, and **6j** were interrogated in U937 and HCT116 at increasing concentrations (1, 5, 10, and 50 µM) up to 48 h of incubation, using both SAHA (*pan* HDAC inhibitor) and PCI (selective HDAC8 inhibitor) as positive controls (Figure S4). These tumor cell lines were chosen since they are representative of hematological and solid tumors and as they show different HDAC6 and HDAC8 expression ratios as previously reported. For selected compounds, the vitality dropped down after 48 h of treatment while after 24 h of induction, no significant effect on cell viability has been highlighted, except at higher concentrations of 10 and 50 µM (Figure S4). At the concentrations of 10 µM all the compounds showed a better activity compared to TUB and PCI used as reference selective HDAC6 and HDAC8 inhibitors, respectively (Figure 5).

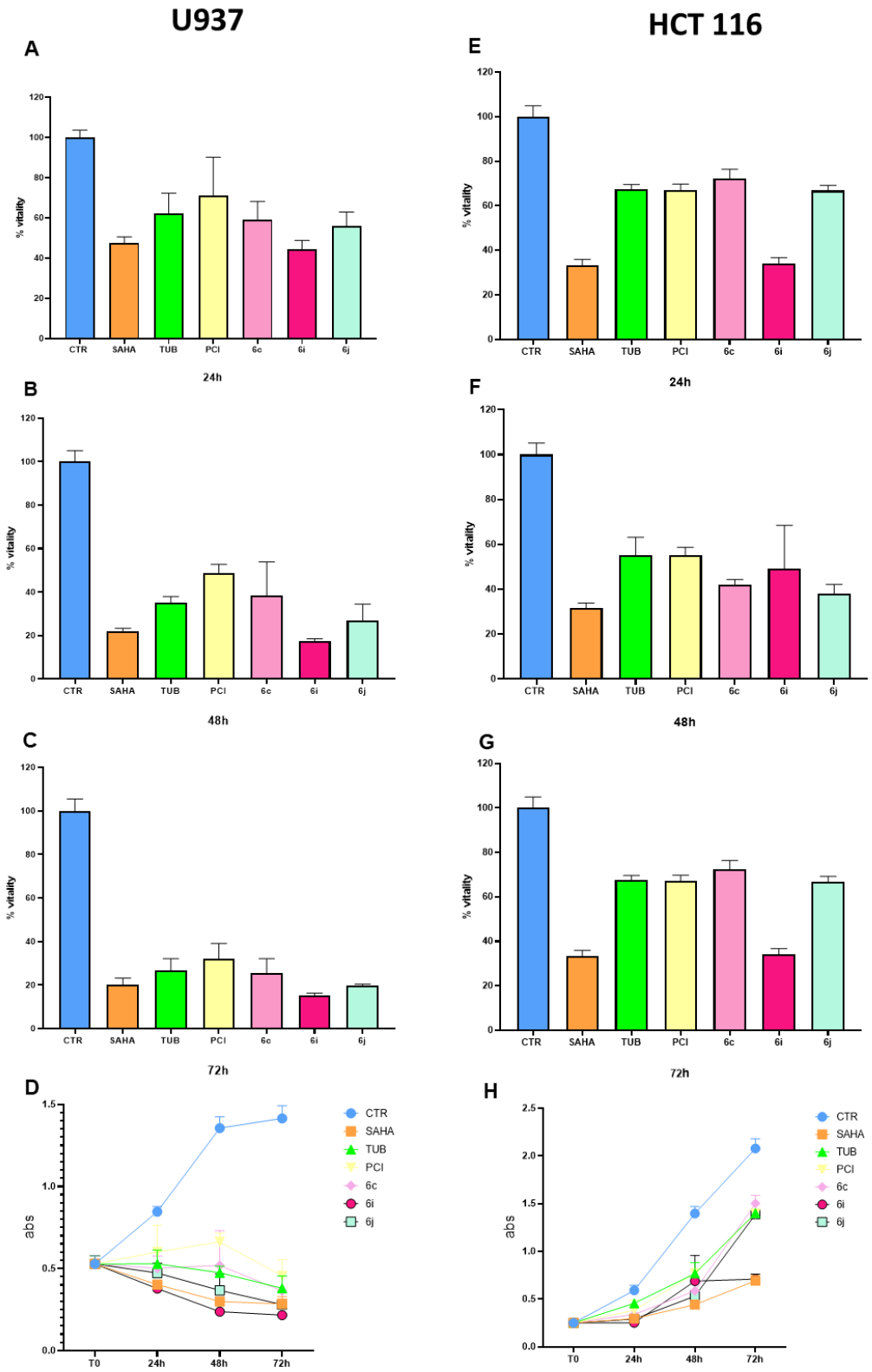

Figure 5. MTT assay results expressed as percentage % of viability in U937 and HCT 116 cells after induction with SAHA (5 µM), TUB (10 µM), PCI (10 µM), **6c** (10 µM), **6i** (10 µM), and **6j** (10 µM), for 24 h ,48 h, and 72 h (A,B,C in U937 cells) and for 24 h, 48 h, and 72 h (E,F,G in HCT 116 cells). Experiments were performed in triplicates. Standard deviations have been reported as error bar. Time course in U937 (D) and HCT 116 (H) cells showing proliferation rate reported as absorbance (abs).

Furthermore, compound **6j** has been also assayed in B cells derived from chronic lymphocytic leukemia affected patients, but no significative reduction in proliferation has been observed, according also with literature data confirming a low expression of these two isoforms in chronic lymphocytic leukemia cells [56] (Figure S5, panels A and B).

*2.5. Preliminary studies to assess solubility, chemical, and metabolic stabilities (***6c,j***) and in silico calculation of specific physicochemical parameters of* **6a-m**

In order to ascertain if these molecules are druggable tools, we measured by HPLC methods the solubility and chemical stability of compounds **6c** and **6j**. Solubility and chemical stability were measured at pH = 7.4 (Table 2); in addition, chemical stability has also been evaluated at pH = 3 and pH = 9.2 (Table S1). The two compounds were sufficiently stable at pH = 7.4, showing a different solubility with **6c** performing better than **6j**. However, the solubility, the chemical stability, and calculated LogP value of these compounds were satisfactory. Furthermore, the compounds were evaluated for their stability under stress conditions (UV = 254 nM or T = 40 °C, after 24 h stress), showing good stability. Noteworthy, compounds **6c** and **6j** also showed favorable LogP values (cLogP<3), that are suitable for predicting absorption after oral administration. These data are also in line with those predicted by computational calculations (see Table 4).

Table 2. Solubility and chemical stability of compounds **6c** and **6j**.

	Solubility (µM) after 24 h	Chemical Stability (%) after 24 h	UV (254 nM)	T = 40 °C	LogP
	pH = 7.4	pH = 7.4			
6c	70	73	100	100	2.75
6j	10	75	100	94	2.78

Furthermore, *in vitro* studies were conducted to assess the metabolic stability of **6c** and **6j** in human (H), mouse (M), and rat (R) liver microsomal (LM) preparations.

Table 3. Kinetic parameters and metabolic stability of **6c** and **6j** in HLM, MLM, and RLM.

	HLM		**MLM**		**RLM**	
	6c	**6j**	**6c**	**6j**	**6c**	**6j**
k (min-^{1})	0.0129	0.0362	0.0109	0.01036	0.0081	0.0071
$t_{1/2}$ (min)	54	19	64	67	86	98
Cl_{int} *(μL/min/mg proteins)*	32.28	90.50	35.38	33.63	8.43	7.39

Data are presented as mean ± SEM of three different experiments.

The plot of non-metabolized compound [natural logarithm of % of compound recovery (100% at time 0 min)] as a function of incubation time showed a mono-exponential decay relationship (first-order kinetics) for both substrates (Figure 7). The apparent decay constant (k) and half-life time ($t_{1/2}$) are reported in Table 3. The incubation of both compounds showed different behaviour as confirmed by the $t_{1/2}$ values. The similar values of intrinsic clearance (Cl_{int}) indicate that both **6c** and **6j** can be considered to possess intermediate properties in terms of metabolic stability, although the data obtained in rat model are extremely different from those observed in human and mouse models.

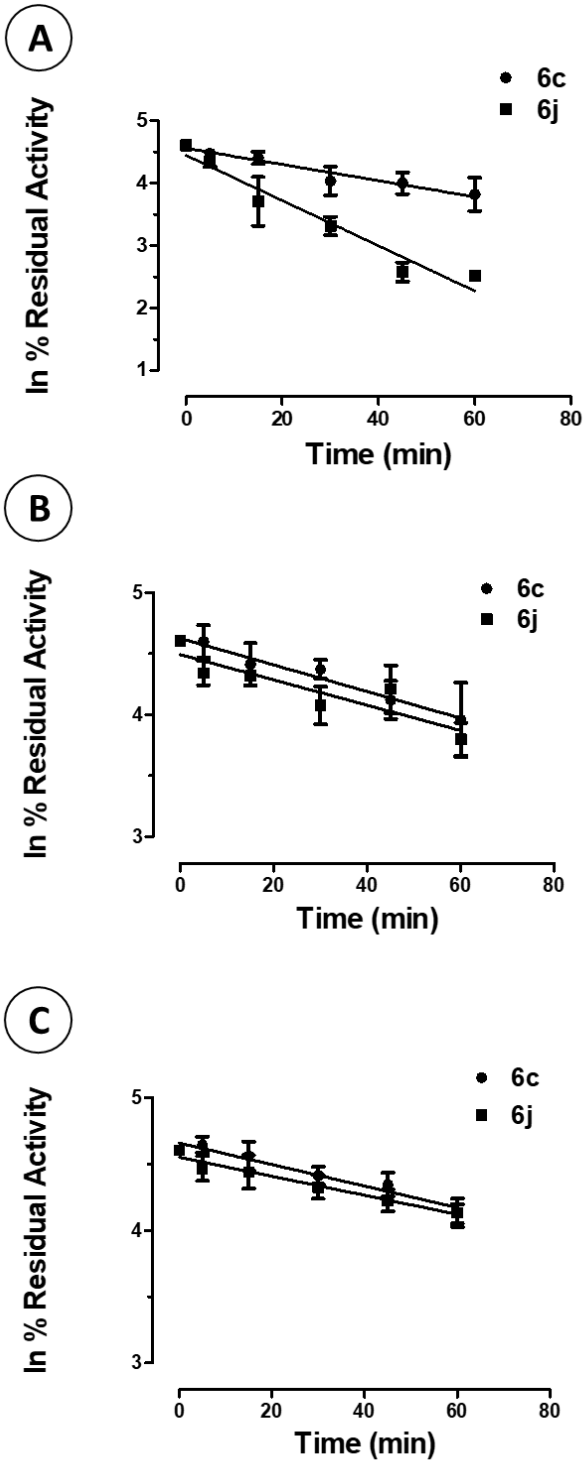

Figure 7. CYP-dependent metabolic depletion of 5 μM **6c** (three time points, at 0, 30, and 60 min) and **6j** (six time points, at 0, 5, 15, 30, 45, and 60 min) in HLM (A), MLM (B), RLM (C) preparations. Results are presented graphically as a percentage of compound recovery (100% at time 0 min) as a function of incubation time. Data are presented as mean ± SEM of three different experiments.

To assess *in silico* further drug-likeness of compounds **6a-m**, we also calculated specific physicochemical properties as reported in Table 4. All the newly developed compounds presented a

topological polar surface area (TPSA) value in a good range that should permit the permeation of the molecule through the membrane of the cells, but not enough to permeate the blood-brain barrier. It is well known that highly hydrophobic compounds could be poorly absorbed and metabolized; moreover, they may also bind to lipophilic targets leading to potential toxicity. For this reason, we predicted the LogP values (cLogP) of our compounds, obtaining extremely spread-out results due to the different polarity of the linker chains used to attach the ZBG to the azetidine-2-one core. Noteworthy, compounds **6c**, **6i** and **6j**, characterized by the best IC_{50} values, showed also good cLogP values (cLogP<3), suitable for absorption after oral ingestion.

Table 4. Calculated physicochemical parameters of compounds **6a-m**

Compod	TPSA	cLogP	Compod	TPSA	cLogP
6a	102	2.83	**6h**	102	2.95
6b	90	2.54	**6i**	90	2.58
6c	102	2.45	**6j**	102	2.49
6d	90	2.94	**6k**	99	3.14
6e	90	3.27	**6l**	102	1.19
6f	90	3.27	**6m**	102	1.14
6g	90	2.94			

2.6. Preliminary toxicity evaluation in mouse fibroblasts

Mouse fibroblast (NIH3T3 cells) were used to study the cytotoxicity of this novel class of selective HDACis (**6b**, **6c**, **6i**, **6j**, **6k**, and **6m)**. The cell viability was determined by the Neutral Red Uptake test and data normalized as % control. TC_{50} values of 48 and 40 µM were observed for compounds **6b**, **6i** and **6j**, respectively. Compounds **6c** and **6k** showed TC_{50} values over 80 µM (Table 5). As a result, these outcomes indicate a safe profile in normal cells for these compounds.

Table 5. TC_{50} (µM) values of **6b**, **6i**, **6j**, **6k**, and **6m** in NIH3T3 cell line.

Compounds	6b	6c	6i	6j	6k	6l	SAHA
TC_{50} (μM)	48	101	48	40	80	100	2.5

Cell viability was measured by the neutral red uptake (NRU) test, and data were normalized as % control. Data are expressed as mean ± s.d. of three experiments repeated in six replicates. *Values are statistically different versus control, $p \leq 0.05$.

*2.7. Evaluation of the toxicity of **6c** and **6j** in zebrafish embryos and their effect on acetylated tubulin*

To provide valuable insights into chemical toxicity of the compounds **6c** and **6j** *in vivo*, we took advantage of the zebrafish model. Zebrafish embryos at 3 days post fertilization (dpf) were treated for 24 h with increasing doses of the compounds dissolved in embryo medium E3 (Figure 6A). Persistent treatments for 48 h did not induce defects as well (data not shown). We chose to start the treatment after the completion of the body axis organization to avoid unspecific effects of the compounds during such a delicate developmental process. Three different concentrations of each compound were tested: 25, 50, and 75 μM. As a control, embryos were treated with the higher concentration of DMSO (75 μM) in which the compounds were dissolved. Both the compounds were well tolerated up to 75 μM, thus confirming their safety profile. Indeed, the general morphology and the anatomical organization of the embryos were comparable between DMSO and **6c** and **6j** treated embryos (Figure 6B-E). The analyses of embryo lethality revealed that there were no significant changes in dead and live embryos among the different categories, thus confirming that these drugs are well tolerated (Figure 6F,H). Moreover, we verified by western blots analyses that the HDAC6/HDAC8 target α-tubulin [57] was increased in the acetylated form following **6c** and **6j** treatments (Figure 6G,I), indicating the efficacy of HDAC inhibition in zebrafish.

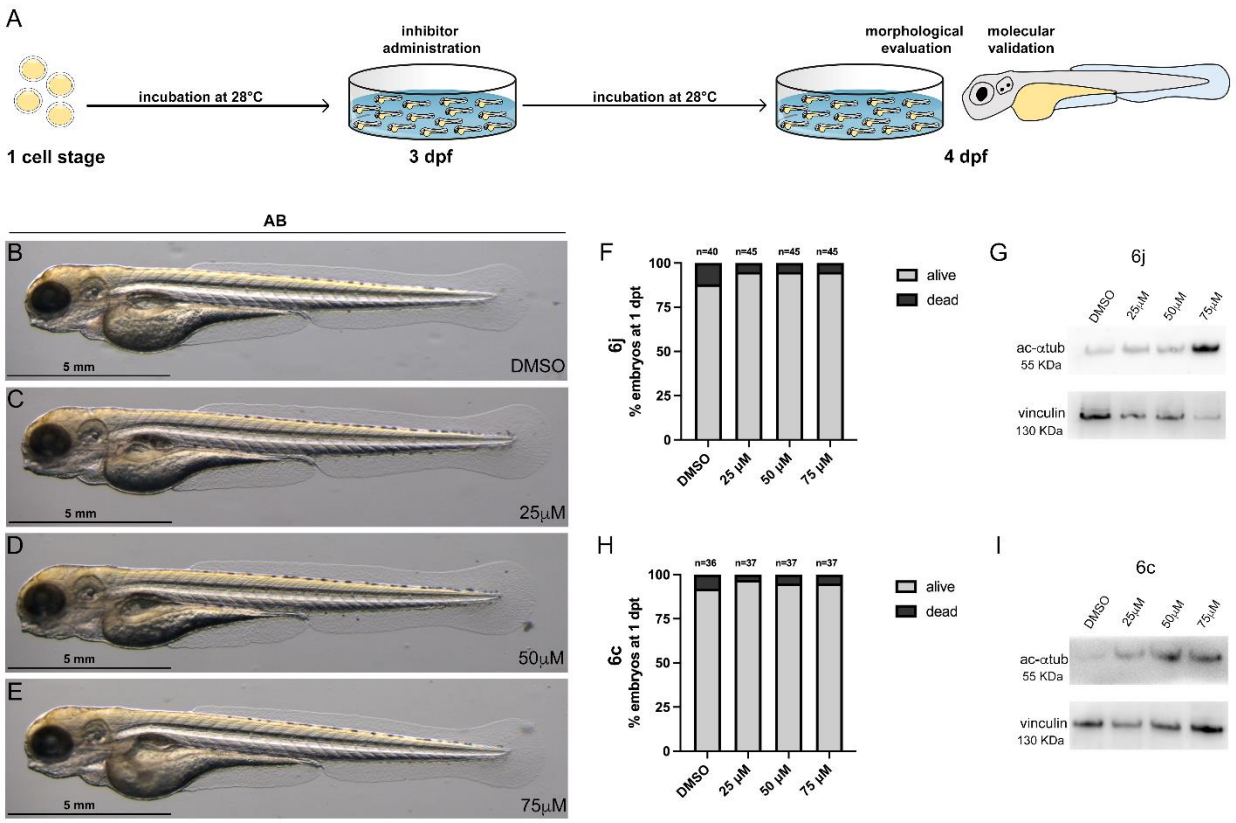

Figure 6. (A) Schematic representation of drug treatments in zebrafish embryos of the wild-type AB strain. (B-E) Toxicity screening of zebrafish embryos treated with different doses (25-75 μM) of **6c** and **6j**.(F, H) in which we show the percentage of embryo lethality after 24 h treatment (1dpi). (G, I) Western blot analyses confirming the efficacy of HDAC inhibition through increased levels of ac-αtubulin compared to the housekeeping vinculin. n = number of embryos.

2.8. Effect of **6j** *in Langendorff perfused rat heart*

To evaluate the cardiotoxic potential of compound **6j**, its effect on cardiac mechanical function and electrocardiogram (ECG) in Langendorff-isolated rat hearts was assessed, as previously described [58]. Under control conditions, LVP and CPP values of 64.4 ± 5.42 and 51.2 ± 0.67 mmHg (n = 4), respectively, were obtained. At the maximum concentration tested (10 μM), **6j** did not affect both LVP and CPP (data not shown) as well as surface ECG (Table 6). In conclusion, **6j** did not affect cardiac parameters up to 10 μM concentration.

Table 6. Effects of **6j** on HR, RR, PQ, QRS, QT, and QTc in Langendorff Perfused Rat Hearts. Each value represents mean ± SEM (n = 4 hearts).

6j (μM)	HR (BPM)	RR (MS)	PQ (MS)	QRS (ms)	QT (ms)	QTc (ms)
none	252.3 ± 10.1	239.5 ± 9.2	45.4 ± 3.9	13.3 ± 0.6	66.1 ± 1.1	66.4 ± 1.3
0.01	251.2 ± 6.7	239.8 ± 5.7	44.4 ± 4.6	12.8 ± 0.4	66.7 ± 1.1	66.9 ± 1.0
0.1	258.4 ± 5.9	233.1 ± 5.1	44.9 ± 4.5	13.1 ± 0.3	66.1 ± 1.5	68.2 ± 0.7
1	252.0 ± 3.4	237.2 ± 2.8	46.2 ± 5.2	13.9 ± 0.4	68.1 ± 1.3	68.9 ± 1.3
10	248.4 ± 3.6	241.5 ± 4.1	47.5 ± 5.2	13.9 ± 0.3	68.5 ± 0.8	68.6 ± 1.4

Each value represents mean ± SEM (n = 5). **$p < 0.01$, repeated measures ANOVA and Dunnett's post-test. HR, frequency; RR, cycle length; PQ, atrioventricular conduction time; QRS, intraventricular conduction time; QT, duration of ventricular depolarization and repolarization, i.e., the action potential duration; QTc, corrected QT.

The toxicity potential of the new HDACis was also assessed and we observed that the compounds exhibit limited cell toxicity both *in vitro* and *in vivo*, while only **6j** compound was tested on Langendorff perfused rat hearts and did not show cardiac toxicity up to 10 μM. Therefore, among the new molecules identified, analogue **6j**, characterized by a 3,3'-diphenylazetidin-2-one cap group, could be considered a prototype hit for dual *h*HDAC6/*h*HDAC8 inhibitors for future explorations.

3. Conclusion

In this study, we developed an interesting new class of *h*HDAC6/*h*HDAC8 inhibitors, based on the azetidine-2-one structure, using the classical pharmacophoric approach for HDACis by combining an innovative cap group, to a linker and a ZBG. In particular, the use of a bulky cap and benzyl linker chain prompted us to discover a new class of *h*HDAC6/*h*HDAC8 dual inhibitors, with no significant effect against *h*HDAC1 and *h*HDAC10. The selectivity of the azetidine-2-one analogues was confirmed in cellular experiments, where the acetylation levels of α-tubulin and SMC3 demonstrated the inhibition of the two targets of interest. HDAC8 unique structural and functional specializations,

together with the recent discovery of HDAC8 involvement in tumorigenesis processes, suggest that *h*HDAC8 alone or *h*HDAC6/8 in combination deserve a thorough investigation as challenging targets in the development of anticancer therapeutics. Compounds **6c**, **6i**, and **6j** with dual *h*HDAC6/*h*HDAC8 inhibitory profile, have demonstrated to hit specifically *h*HDAC6 and *h*HDAC8 targets in hematological and in solid cancers. Compounds **6c,i,j** represent an example of potent dual acting *h*HDAC6/8 inhibitors and their potential will be further investigated.

4. Experimental section

4.1. General remarks

All chemicals and reagents were purchased from the commercial suppliers and used without further purification, unless and otherwise specified. Reaction progress was observed by thin-layer chromatography (TLC), carried out on silica (60 F254) or alumina (60 F254, basic) gel plates with detection by UV and the products were purified by means of either silica (60M, 0.040-0.063 μm) or alumina (90, standardized) column chromatography. ^{1}H and ^{13}C NMR spectra were documented in the indicated deuterated solvent on a Varian 300 MHz or a Bruker 400 MHz spectrometer by using the residual signal of the deuterated solvent as internal standard. Splitting patterns are indicated by s (singlet), d (doublet), dd (doublet of doublets), t (triplet), q (quartet), m (multiplet), and br (broad); chemical shifts (δ) are defined in parts per million (ppm) and coupling constants (J) in Hertz (Hz). ESI-MS spectra were performed by an Agilent 1100 Series LC/MSD spectrometer. HRESIMS were carried out by a Thermo Finningan LCQ Deca XP Max ion-trap mass spectrometer equipped with Xcalibur software, operated in positive ion mode, and conducted at the University of Naples, Italy. Yields denote to purified products. HPLC analysis were performed with a Shimadzu Prominence apparatus equipped with a scanning absorbance UV-VIS detector (Diode Array SPD-M20A) also equipped with a thermostatic chamber and Purospher®STAR, RP-18ε (5 μM) HPLC column. All

moisture-sensitive reactions were executed under nitrogen atmosphere using oven-dried glassware and freshly distilled dry solvents.

4.2.1. trans-1-(1-Benzylpiperidin-4-yl)-3,4-diphenylazetidin-2-one ((±)-**8**). A solution of phenylacetic acid (1072 mg, 15.75 mmol) and triphosgene (778 mg, 2.63 mmol) in dry DCM (30 mL) was heated at 50 °C for 30 min. Then, a solution of **7** (1461 mg, 5.25 mmol) in dry DCM (30 mL) was added dropwise, followed by the addition of TEA (2.2 mL, 15.75 mmol) and the mixture was heated at 50 °C for 12 h. The solvent was removed under reduced pressure and the crude was purified by flash-chromatography on silica gel (EtOAc:PE 1:2), yielding ((±)-**8**) as a yellow oil. 65% yield. ^{1}H NMR (300 MHz, $CDCl_3$) δ 7.53-7.11 (m, 15H), 4.53 (d, J = 2.2 Hz, 1H), 4.11 (d, J = 2.0 Hz, 1H), 3.64 (m, 1H), 3.47 (s, 2H), 2.84 (dd, J = 43.4, 11.4 Hz, 2H), 2.01 (m, 4H), 1.72 (dd, J = 12.8, 3.1 Hz, 1H), 1.56-1.50 (m, J = 11.7, 4.0 Hz, 1H). ESI-MS *m/z*: 397 $[M+H]^+$, 419 $[M+Na]^+$.

4.2.2. trans-3,4-Diphenyl-1-(piperidin-4-yl)azetidin-2-one ((±)-**9**). To a solution of (±)-**8** (100 mg, 0.25 mmol) in methanol (2.5 mL) was added a catalytic amount of Pd-C and the mixture was gently charged from N_2 to H_2 atmosphere. After 12 h, the mixture was filtered, and the liquid residue evaporated to obtain the final compound in quantitative yield as a yellow oil. ^{1}H NMR (300 MHz, CD_3OD) δ 1H NMR (300 MHz, CDCl3) δ 7.45 – 7.20 (m, 10H), 4.51 (d, J = 2.2 Hz, 1H), 4.10 (d, J = 2.2 Hz, 1H), 3.75 – 3.61 (m, 1H), 3.09 (dt, J = 12.8, 3.7 Hz, 1H), 2.96 (dt, J = 12.7, 3.9 Hz, 1H), 2.67 – 2.45 (m, 2H), 2.08 – 1.94 (bs, 1H), 1.89 – 1.66 (m, 2H), 1.43 – 1.26 (m, 1H). ESI-MS *m/z*: 307 $[M+H]^+$.

4.2.3. General procedure for the synthesis of ureas (±)-**10a**,**c**, and **h**. A solution of (±)-**9** (0.15 mmol) in dry THF (0.8 mL) was added to a solution of the appropriate isocyanate (2 eq.) in dry THF (0.8 mL), followed by the addition of TEA (4 eq.). The reaction mixture was then heated at 65 °C for 1.5

h. Solvent was removed under reduced pressure and the crude was purified by silica gel column chromatography (PE:EtOAc 2:1) to afford the corresponding compounds.

4.2.3.1. trans-Methyl 4-(4-(2-oxo-3,4-diphenylazetidin-1-yl)piperidine-1-carboxamido)benzoate ((±)-**10a**). Following the general procedure for the synthesis of ureas, the title compound was obtained by reacting (±)-**9** with methyl 4-isocyanatobenzoate, prepared as previously reported [39]. Light yellow oil, 59% yield. ^{1}H-NMR (300 MHz, $CDCl_3$) δ 7.90 (d, J = 8.4 Hz, 2H), 7.49-7.18 (m, 12H), 4.50 (s, 1H), 4.13-3.90 (m, 3H), 3.86 (s, 3H), 3.65 (t, J = 10.7 Hz, 1H), 2.88 (dd, J = 26.8, 12.8 Hz, 2H), 2.10-1.40 (m, 4H). ESI-MS *m/z*: 484 $[M+H]^+$.

4.2.3.2. trans-Methyl 4-((4-(2-oxo-3,4-diphenylazetidin-1-yl)piperidine-1-carboxamido)methyl)benzoate ((±)-**10c**). Following the general procedure for the synthesis of ureas, the title compound was obtained by reacting (±)-**9** with methyl 4-(isocyanatomethyl)benzoate, prepared as previously reported [20]. White solid, 95% yield. ^{1}H NMR (300 MHz, CD_3OD) δ 7.99-7.86 (m, 2H), 7.49-7.20 (m, 12H), 4.64 (t, J = 4.9 Hz, 1H), 4.35 (s, 2H), 4.12 (t, J = 2.8 Hz, 1H), 4.08-3.85 (m, 5H), 3.71-3.65 (m, 1H), 2.96-2.70 (m, 2H), 2.05-1.70 (m, 2H), 1.57-1.23 (m, 2H). ESI-MS *m/z*: 498 $[M+H]^+$.

4.2.3.3. trans-Methyl 2-(4-(4-(2-oxo-3,4-diphenylazetidin-1-yl)piperidine-1-carboxamido)phenyl)acetate ((±)-**10h**). Following the general procedure for the synthesis of ureas, the title compound was obtained by reacting (±)-**9** with methyl 2-(4-isocyanatophenyl)acetate, prepared as previously reported [43]. White solid, 85% yield. ^{1}H NMR (300 MHz, CD_3OD) δ 7.97-7.87 (m, 2H), 7.48-7.20 (m, 10H), 7.13-6.99 (m, 2H), 4.69-4.61 (m, 1H), 4.37-4.31 (m, 2H), 4.14-4.08 (m, 1H), 4.07-3.96 (m, 1H), 3.91-3.82 (m, 4H), 2.86-2.80 (m, 2H), 2.05-1.69 (m, 3H), 1.44-1.36 (m, 2H). ESI-MS *m/z*: 498 $[M+H]^+$.

4.2.4. General procedure for the synthesis of amides (±)-**10b**,**d-g**. The appropriate carboxylic acid (1 eq.) was dissolved in dry DCM (3 mL), under N_2 and then EDCI (1.2 eq.), HOBt (1.5 eq.) and DIPEA (4 eq.) were added at 0 °C. The suspension was stirred at 0 °C for 15 min, then a solution of (±)-**9** (0.151 mmol, 1 eq.) in dry DCM (3 mL) was added. The reaction was stirred at 25 °C for 12 h. Subsequently, the mixture was washed with NH_4Cl (s.s.) and then with $NaHCO_3$ (s.s.). The organic layers were combined, washed with brine, dried over anhydrous Na_2SO_4, filtered, and evaporated under reduced pressure. The crude product was purified by silica gel column chromatography (DCM:acetone 30:1 to 10:1) to give the corresponding compounds.

4.2.4.1. trans-Ethyl 4-(2-oxo-2-(4-(2-oxo-3,4-diphenylazetidin-1-yl)piperidin-1-yl)ethyl)benzoate ((±)-**10b**). Following the general procedure for the synthesis of amides, the title compound was obtained by reacting (±)-**9** with 2-(4-(methoxycarbonyl)phenyl)acetic acid, prepared as previously reported [20]. White solid, 56% yield. ^{1}H NMR (300 MHz, $CDCl_3$) δ 7.95 (m, 2H), 7.47-7.13 (m, 12H), 4.59 (d, J = 13.7 Hz, 1H), 4.48-4.27 (m, 4H), 4.11 (s, 1H), 3.76 (m, 4H), 3.13-2.83 (m, 1H), 2.76-2.57 (m, 1H), 1.94 (m, 1H), 1.80-1.54 (m, 2H), 1.39 (t, J = 9.7 Hz, 3H). ESI-MS *m/z*: 497 $[M+H]^+$

4.2.4.2. trans-Ethyl 3-(4-(4-(2-oxo-3,4-diphenylazetidin-1-yl)piperidine-1-carbonyl)phenyl)propanoate ((±)-**10d**). Following the general procedure for the synthesis of amides, the title compound was obtained by reacting (±)-**9** with 4-(3-ethoxy-3-oxopropyl)benzoic acid, prepared as previously reported [40]. White solid, 29% yield. ^{1}H NMR (300 MHz, $CDCl_3$) δ 7.51-7.18 (m, 14H), 4.54 (s, 1H), 4.23-4.07 (m, 3H), 3.85-3.68 (m, 2H), 3.12-2.83 (m, 4H), 2.63 (t, J = 7.6 Hz, 2H), 2.19-1.69 (m, 4H), 1.63-1.40 (s, 1H), 1.25 (t, J = 7.2 Hz, 3H). ESI-MS *m/z*: 511 $[M+H]^+$.

4.2.4.3. trans-Methyl (E)-4-(3-oxo-3-(4-(2-oxo-3,4-diphenylazetidin-1-yl)piperidin-1-yl)prop-1-en-1-yl)benzoate ((±)-**10e**). Following the general procedure for the synthesis of amides, the title

compound was obtained by reacting (±)-**9** with *trans*-3-(4-(methoxycarbonyl)phenyl)acrylic acid, prepared as previously reported [42]. White solid, 68% yield. ^{1}H NMR (300 MHz, CD_3OD) δ 7.95 (d, J = 7.9 Hz, 2H), 7.66-7.56 (m, 2H), 7.50 (d, J = 15.4 Hz, 1H), 7.43-7.14 (m, 9H), 4.64 (d, J = 2.0 Hz, 1H), 4.43 (dd, J = 39.0, 12.4 Hz, 1H), 4.26-4.03 (m, 2H), 3.85 (s, 3H), 3.77-3.63 (m, 1H), 3.26-3.04 (m, 1H), 2.88-2.67 (m, 1H), 2.17-1.74 (m, 4H), 1.60-1.37 (m, 2H). ESI-MS *m/z*: 495 $[M+H]^+$.

4.2.4.4. trans-ethyl-3-(4-(4-(2-oxo-3,4-diphenylazetidin-1-yl)piperidine-1-carbonyl)phenyl)acrylate ((±)-**10f**). Following the general procedure for the synthesis of amides, the title compound was obtained by reacting (±)-**9** with trans-4-(3-ethoxy-3-oxoprop-1-en-1-yl)benzoic acid, prepared as previously reported [40]. White solid, 65% yield. ^{1}H NMR (300 MHz, CD_3OD) δ 7.73-7.56 (m, 3H), 7.53-7.17 (m, 11H), 4.67 (d, J = 2.0 Hz, 1H), 4.53-4.42 (m, 1H), 4.23 (q, J = 7.1 Hz, 2H), 4.12 (d, J = 2.0 Hz, 1H), 3.78-3.49 (m, 2H), 3.18-2.77 (m, 2H), 2.21-1.65 (m, 4H), 1.65-1.41 (m, 2H), 1.30 (t, J = 7.1 Hz, 3H). ESI-MS *m/z*: 509 $[M+H]^+$.

4.2.4.5. trans-Methyl 4-(3-oxo-3-(4-(2-oxo-3,4-diphenylazetidin-1-yl)piperidin-1-yl)propyl)benzoate ((±)-**10g**). Following the general procedure for the synthesis of amides, the title compound was obtained by reacting (±)-**9** with 3-(4-(methoxycarbonyl)phenyl)propanoic acid, prepared as previously reported [59]. White solid, 60% yield. ^{1}H NMR (300 MHz, $CDCl_3$) δ 7.46-7.07 (m, 14H), 4.51 (s, 1H), 4.13 (s, 1H), 3.85 (s, 3H) 3.76-3.58 (m, 1H), 3.15-2.71 (m, 4H), 2.38-2.17 (m, 2H), 2.12-1.86 (m, 2H), 1.85-1.33 (m, 4H). ESI-MS *m/z*: 497 $[M+H]^+$.

4.2.5. Dimethyl (1-benzylpiperidin-4-yl)carbonimidodithioate (**12**). A solution of 20 M aqueous NaOH (10mL) was added to 1-benzylpiperidin-4-amine (**11**) (1 g, 5.26 mmol) at 0 °C and stirred for 5 min; then, a solution of carbon disulfide (400 mg, 5.26 mmol) in toluene (3 mL) was added to the reaction mixture, followed by a fast addition of a solution of methyl iodide (983 μL, 15.78 mmol) in toluene (3 mL) at 25 °C and stirred for another 5 min. After that, benzyltriethylammonium chloride

(120 mg, 0.53 mmol) was added to the reaction mixture and stirred for another 30 min. Toluene was removed under reduced pressure. The crude was dissolved in Et_2O, washed with H_2O, dried over anhydrous Na_2SO_4, filtered, and concentrated to obtain the compound in quantitative yield which was used in the next step without any further purification. ^{1}H NMR (300 MHz, $CDCl_3$) δ 7.44-7.28 (m, 5H), 3.79-3.63 (m, 1H), 3.53 (d, J = 10.2 Hz, 2H), 2.91-2.78 (m, 2H), 2.55 (s, 3H), 2.37 (s, 3H), 2.30-2.11 (m, 2H), 1.88-1.61 (m, 4H); ESI-MS *m/z*: 295 $[M+H]^+$.

4.2.6. 1-(1-Benzylpiperidin-4-yl)-4,4-bis(methylthio)-3,3-diphenylazetidin-2-one (**13**). Triphosgene (227 mg, 0.76 mmol) was added to a solution of **12** (486 mg, 2.29 mmol) in dry DCM (9.3 mL); then, it was heated at 50 °C for 30 min. A solution of diphenylacetic acid (450 mg, 1.53 mmol) in dry DCM (9.3 mL) and TEA (640 μL, 4.59 mmol) were added to the reaction mixture and refluxed for 12 h. A satured solution of $NaHCO_3$ was added slowly to the cooled mixture at rt and the compound was extracted with DCM (3 x 15 mL). The combined organic layers were dried over anhydrous Na_2SO_4, filtered, and concentrated under reduced pressure. The residue was purified by silica gel column chromatography (DCM:Acetone 40:1) to afford the title compound **13**. Yellow oil, 52% yield. ^{1}H NMR (300 MHz, $CDCl_3$) δ 7.73 (d, J = 7.0 Hz, 4H), 7.42-7.20 (m, 11H), 3.54 (s, 2H), 3.27 (dt, J = 19.8, 7.9 Hz, 1H), 3.00 (d, J = 11.7 Hz, 2H), 2.66-2.46 (m, 2H), 2.11-1.92 (m, 4H), 1.73 (s, 6H); ESI-MS *m/z*: 489 $[M+H]^+$.

4.2.7. 1-(1-Benzylpiperidin-4-yl)-3,3-diphenylazetidin-2-one (**14**). Nickel (II) chloride hexahydrate (730 mg, 3.07 mmol) and $NaBH_4$ (348 mg, 9.21 mmol) was added to a solution of **13** (300 mg, 0.61 mmol) in methanol (32 mL) and THF (8 mL) at 25 °C and stirred for 2 h. After that, the reaction was quenched with a slow addition of H_2O, extracted with EtOAc, dried over anhydrous Na_2SO_4, filtered, and concentrated under reduced pressure. The residue was purified by silica gel column chromatography (PE:EtOAc 1:1) to afford the title compound **14**. Yellow oil, 35% yield. ^{1}H NMR

(300 MHz, $CDCl_3$) δ 7.49-7.16 (m, 15H), 3.85 (s, 2H), 3.82-3.67 (m, 1H), 3.50 (s, 2H), 2.90 (d, J = 12.0 Hz, 2H), 2.10-2.04 (m, 2H), 1.93-1.63 (m, 4H). ESI-MS *m/z*: 397 $[M+H]^+$.

4.2.8. 3,3-Diphenyl-1-(piperidin-4-yl)azetidin-2-one (**15**). Following the same procedure described for the synthesis of (±)-**9**, compound **15** was synthesized starting from **14**. Yellow oil, quantitative yield. ^{1}H NMR (300 MHz, CD_3OD) δ 7.43 – 7.20 (m, 10H), 3.98 (s, 2H), 3.95 – 3.82 (m, 1H), 3.40 (dt, J = 13.3, 3.9 Hz, 2H), 3.08 (td, J = 12.9, 3.4 Hz, 2H), 2.21 – 1.93 (m, 4H).

4.2.9. Methyl 4-(2-oxo-2-(4-(2-oxo-3,3-diphenylazetidin-1-yl)piperidin-1-yl)ethyl)benzoate (**16a**). The title compound was prepared following the same procedure described for compound (±)-**10b**. White solid, 60% yield. ^{1}H NMR (300 MHz, $CDCl_3$) δ 8.03-7.94 (m, 2H), 7.43-7.15 (m, 12H), 4.52 (d, J = 13.5 Hz, 1H), 3.95-3.86 (m, 3H), 3.84-3.79 (m, 2H), 3.79-3.70 (m, 3H), 3.16-2.99 (m, 1H), 2.94-2.69 (m, 1H), 1.85 (t, J = 14.4 Hz, 3H), 1.67-1.31 (m, 2H). ESI-MS *m/z*: 483 $[M+H]^+$.

4.2.10. Methyl 4-((4-(2-oxo-3,3-diphenylazetidin-1-yl)piperidine-1-carboxamido)methyl)benzoate (**16b**). The title compound was prepared following the same procedure described for compound (±)-**10c**. White solid, yield 96%. ^{1}H NMR (300 MHz, CD_3OD) δ 7.93 (d, J = 8.0 Hz, 2H), 7.41-7.13 (m, 12H), 4.42-4.30 (m, 2H), 3.98 (t, J = 15.9 Hz, 2H), 3.92-3.83 (m, 5H), 3.83-3.69 (m, 1H), 2.96-2.81 (m, 2H), 1.94-1.50 (m, 4H). ESI-MS *m/z* 498 $[M+H]^+$.

4.2.11. 4-(methoxycarbonyl)benzyl 4-(2-oxo-3,3-diphenylazetidin-1-yl)piperidine-1-carboxylate (**16c**). To a solution of **15** (100 mg, 0.33 mmol) in DCM (4 mL) at 0 °C, CDI (53 mg, 0.33 mmol) and methyl 4-(hydroxymethyl)benzoate (65 mg, 0.40 mmol), prepared as previously reported [47], were added. The mixture was warmed to 25 °C and stirred for 6 h, then H_2O was added and phases were separated. Organic phase was concentrated under reduced pressure and the crude was purified by silica gel column chromatography (PE:EtOAc 2:1) to afford the title compound. White solid, 65%

yield. ^{1}H NMR (300 MHz, $CDCl_3$) δ 8.08-7.97 (m, 2H), 7.47-7.17 (m, 12H), 5.17 (s, 2H), 4.25-4.10 (m, 2H), 3.93-3.90 (m, 3H), 3.90-3.85 (m, 1H), 3.84-3.80 (m, 2H), 3.05-2.80 (s, 2H), 1.99-1.83 (m, 2H), 1.72-1.55 (m, 2H). ESI-MS *m/z* 498 $[M+H]^+$.

4.3.1. (±)-tert-Butyl 4-((3-methoxy-3-oxo-1-(m-tolyl)propyl)amino)piperidine-1-carboxylate ((±)-**18a**). To a solution of methyl 3-amino-3-(*m*-tolyl) propanoate (962 mg, 4.18 mmol) in DMF (8.4 mL), DIPEA (4.2 mL, 23.8 mmol), AcOH (422 µL, 71.06 mmol), and then *N*-Boc-piperidone (957 mg, 4.80 mmol) were added. The mixture was stirred at 25 °C for 12 h and then $NaBH_3CN$ (604 mg, 9.61 mmol) was added. After 12 h the reaction was quenched with $NaHCO_3$ (s.s.) and extracted with EtOAc (3 x 10 mL). The combined organic phases were dried over Na_2SO_4, filtered and concentrated under reduced pressure. The crude was purified by silica gel column chromatography (PE:EtOAc 2:1) to afford the title compound. White solid, 53% yield. ^{1}H NMR (300 MHz, $CDCl_3$) δ 7.20 (d, *J* = 7.5 Hz, 1H), 7.13-7.01 (m, 3H), 4.23-4.14 (m, 1H), 4.00-3.78 (br, 2H), 3.64 (s, 3H), 2.83-2.63 (m, 2H), 2.62-2.54 (m, 2H), 2.49-2.38 (m, 1H), 2.34 (s, 3H), 1.89 (d, *J* = 13.0 Hz, 1H), 1.68-1.53 (m, 1H), 1.42 (s, 9H), 1.29-1.14 (m, 2H). ESI-MS *m/z*: 377 $[M+H]^+$.

4.3.2. (±)-tert-Butyl 4-((1-(3-chlorophenyl)-3-methoxy-3-oxopropyl)amino)piperidine-1-carboxylate ((±)-**18b**). Starting from methyl 3-amino-3-(3-chlorophenyl)propanoate (1.160 g, 4.65 mmol), title compound was obtained following the procedure described for the preparation of (±)-**18a**. Purification by silica gel column chromatography (PE:EtOAc 3:1) afforded the title compound as a yellow oil, 33% yield. ^{1}H NMR (300 MHz, $CDCl_3$) δ 7.36-7.29 (m, 1H), 7.27-7.13 (m, 3H), 4.21 (t, *J* = 8.0, 5.9 Hz, 1H), 4.01-3.76 (br, 2H), 3.65 (s, 3H), 2.80-2.63 (m, 2H), 2.61-2.51 (m, 2H), 2.45-2.32 (m, 1H), 1.88 (d, *J* = 12.9 Hz, 1H), 1.61 (d, *J* = 12.7 Hz, 1H), 1.40 (s, 9H), 1.30-1.16 (m, 2H). ESI-MS *m/z*: 397 $[M+H]^+$.

4.3.3. (±)-tert-Butyl (R)-4-(2-oxo-4-(m-tolyl)azetidin-1-yl)piperidine-1-carboxylate ((±)-**19a**). To a solution of (±)-**18a** (377 mg, 1.10 mmol, 1.0 eq.) in a mixture of THF/MeOH/H_2O (1:1:1, 3 mL), LiOH (120 mg, 5.01 mmol) was added. The mixture was stirred at 25 °C for 12 h and then the reaction was quenched with 1N HCl solution, until neutral pH. After that, the resulting suspension was extracted with EtOAc (3 x 5 mL) and the combined organic phases were dried over Na_2SO_4, filtered, and concentrated under reduced pressure. The crude was suspended in CH_3CN and 2-chloro-1-methylpyridinium iodide (255 mg, 2.5x mmol) and TEA (696 µL, 5.0x mmol) were added. The resulting mixture was heated to 85 °C for 12 h. After that, solvent was removed under reduced pressure, the residue was dissolved in EtOAc and washed with $NaHCO_3$ (s.s.). The organic phase was dried over Na_2SO_4, filtered, and concentrated under reduced pressure. The crude was purified by silica gel column chromatography (PE:EtOAc 2:1) to afford the title compound as a yellow oil, 41% yield. ^{1}H NMR (300 MHz, $CDCl_3$) δ 7.32-7.20 (m, 2H), 7.13 (d, J = 6.6 Hz, 2H), 4.55-4.47 (m, 1H), 4.13-3.84 (m, 2H), 3.62-3.46 (br, 1H), 3.32-3.28 (m, 1H), 2.82-2.54 (m, 3H), 2.36 (s, 3H), 1.95-1.79 (m, 1H), 1.69-1.50 (m, 3H), 1.40 (s, 9H). ESI-MS *m/z*: 345 $[M+H]^+$.

4.3.4. (±)-tert-Butyl (R)-4-(2-(3-chlorophenyl)-4-oxoazetidin-1-yl)piperidine-1-carboxylate ((±)-**19b**). The title compound was obtained from (±)-**18b** (95 mg, 0.248 mmol) following the procedure described for the preparation of (±)-**19a**. Purification by silica gel column chromatography (PE:EtOAc 2:1) afforded the title compound as a yellow oil, 39% yield. ^{1}H NMR (300 MHz, $CDCl_3$) δ 7.33 (s, 1H), 7.25-7.04 (m, 3H), 4.25-4.00 (m, 1H), 3.99-3.69 (br, 2H), 2.66-2.18 (m, 4H), 1.92-1.71 (br, 1H), 1.61-1.02 (m, 13H). ESI-MS *m/z*: 365 $[M+H]^+$.

4.3.5. (±)-1-(Piperidin-4-yl)-4-(m-tolyl)azetidin-2-one (**20a**). To solution of (±)-**19a** (53 mg, 0.15 mmol) in dry DCM (1.5 mL), TFA (34 µL, 0.45 mmol) was added dropwise at 0 °C under N_2 atmosphere. The mixture was allowed to reach 25 °C and stirred for 1 h, then it was quenched and extracted with $NaHCO_3$ (s.s.). The organic phase was washed with brine, dried over Na_2SO_4, filtered,

and concentrated under reduced pressure to afford the title compound as a yellow oil without further purification (quantitative yield). ^{1}H NMR (300 MHz, $CDCl_3$) δ 8.09-8.04 (m, 1H), 7.29-7.18 (m, 1H), 7.15-7.06 (m, 3H), 4.65 (s, 1H), 4.52 (dd, *J* = 5.2, 2.3 Hz, 1H), 3.62-3.44 (m, 1H), 3.27 (dd, *J* = 14.7, 5.2 Hz, 1H), 3.05 (d, *J* = 12.5 Hz, 1H), 2.93 (d, *J* = 12.5 Hz, 1H), 2.75 (dd, *J* = 14.7, 2.4 Hz, 1H), 2.55-2.50 (m, 2H), 2.34 (s, 3H), 1.94-1.84 (m, 1H), 1.72-1.59 (m, 2H). ESI-MS *m/z*: 245 $[M+H]^+$.

4.3.6. (±)-4-(3-chlorophenyl)-1-(piperidin-4-yl)azetidin-2-one ((±)-**20b**). Starting from (±)-**19b** (70 mg, 0.19 mmol), the title compound was obtained following the procedure described for the preparation of (±)-**20a**, quantitative yield. ^{1}H NMR (300 MHz, $CDCl_3$) δ 8.04 (s, 1H), 7.34-7.29 (m, 1H), 7.29-7.18 (m, 3H), 4.63 (s, 1H), 4.52 (dd, *J* = 5.3, 2.3 Hz, 1H), 3.28 (dd, *J* = 14.7, 5.3 Hz, 1H), 3.03 (d, *J* = 12.7 Hz, 1H), 2.92 (d, *J* = 12.7 Hz, 1H), 2.71 (dd, *J* = 14.7, 2.3 Hz, 1H), 2.60-2.40 (m, 2H), 2.40-2.30 (br, 1H), 1.87 (d, *J* = 13.3 Hz, 1H), 1.65 (dd, *J* = 12.1, 4.0 Hz, 2H). ESI-MS *m/z*: 265 $[M+H]^+$.

4.3.7 (±)-Methyl-4-((4-(2-oxo-4-(m-tolyl)azetidin-1-yl)piperidine-1-carboxamido)methyl)benzoate ((±)-**21a**). Following the general procedure for the synthesis of ureas, starting from (±)-**20a**, the title compound was obtained as a white solid, 39% yield. ^{1}H NMR (300 MHz, $CDCl_3$) δ 7.95 (d, *J* = 8.3 Hz, 2H), 7.34-7.19 (m, 4H), 7.18-7.06 (m, 2H), 4.94-4.81 (m, 1H), 4.52 (dd, *J* = 5.3, 2.3 Hz, 1H), 4.41 (d, *J* = 5.6 Hz, 1H), 4.01-3.85 (m, 4H), 3.85-3.71 (m, 1H), 3.68-3.49 (m, 1H), 3.29 (dd, *J* = 14.8, 5.2 Hz, 1H), 2.91-2.66 (m, 3H), 2.35 (s, 3H), 1.98-1.87 (m, 1H), 1.86-1.62 (m, 2H), 1.37-1.30 (m, 2H). ESI-MS *m/z*: 436 $[M+H]^+$.

4.3.8. (±)-Methyl-4-((4-(2-(3-chlorophenyl)-4-oxoazetidin-1-yl)piperidine-1-carboxamido)methyl)benzoate ((±)-**21b**). Following the general procedure for the synthesis of ureas, starting from (±)-**20b**, the title compound was obtained as a white solid, 60% yield. ^{1}H NMR (300 MHz, $CDCl_3$) δ 7.94 (d, *J* = 8.2 Hz, 2H), 7.39-7.15 (m, 6H), 5.28 (s, 1H), 5.00 (t, *J* = 5.7 Hz, 1H),

4.56-4.45 (m, 1H), 4.39 (d, *J* = 5.6 Hz, 2H), 3.88 (s, 5H), 3.66-3.48 (m, 1H), 3.30 (dd, *J* = 14.8, 5.3 Hz, 1H), 2.86-2.65 (m, 3H), 1.98-1.84 (m, 1H), 1.83-1.61 (m, 2H). ESI-MS *m/z*: 456 $[M+H]^+$.

4.4. General procedure for the synthesis of final compounds **6a-m**. To a solution of the appropriate ester **10a-h**, **16a-c**, and **21a-b** (0.50 mmol) in DCM (2 mL) and methanol (4 mL) at 25 °C, NH_2OH (50 wt. % in H_2O) (100 eq.) was added, followed by a dropwise addition of methanolic KOH (50 eq.) solution and the reaction mixture was stirred for 2 h. After that, a solution of 1 N HCl was added to the reaction mixture until neutral pH. The solvent was removed under reduced pressure and the residue was purified by silica gel column chromatography (DCM/MeOH/NH_4OH 10:1:0.1) to afford the final compound.

4.4.1. trans-N-(4-(hydroxycarbamoyl)phenyl)-4-(2-oxo-3,4-diphenylazetidin-1-yl)piperidine-1-carboxamide ((±)-**6a**). Following the general procedure for the synthesis of the final compounds, title compound was obtained as a white solid, 67% yield, mp 131-133 °C, R_f 0.34 (DCM:MeOH, 9:1). ^{1}H NMR (300 MHz, CD_3OD) δ 7.90 (d, *J* = 8.1 Hz, 1H), 7.65 (d, *J* = 8.2 Hz, 1H), 7.49-7.18 (m, 12H), 4.69 (s, 1H), 4.18-3.99 (m, 3H), 3.73 (m, 1H), 2.95 (dd, *J* = 27.6, 13.3 Hz, 2H), 2.11-1.42 (m, 4H). ^{13}C NMR (75 MHz, CD_3OD) δ 169.6, 155.6, 155.5, 143.3, 138.3, 134.8, 130.1, 128.8, 128.6, 128.6, 127.4, 127.3, 127.1, 126.5, 125.6, 119.2, 118.8, 63.9, 63.2, 51.1, 42.9, 42.7, 30.0, 29.6. ESI-MS *m/z*: 507 $[M+Na]^+$. HRMS (ESI) *m/z* $[M+Na]^+$ calculated for $C_{28}H_{28}N_4NaO_4$ 507.2008 found 507.2009. HPLC Rt (min): 17.82. IR v_{max} 3248, 2926, 2853, 1743, 1645, 1604, 1521 cm^{-1}.

4.4.2. trans-N-hydroxy-4-(2-oxo-2-(4-(2-oxo-3,4-diphenylazetidin-1-yl)piperidin-1-yl)ethyl)benzamide ((±)-**6b**). Following the general procedure for the synthesis of the final compounds, title compound was obtained as an orange solid, 24% yield, mp 127-129 °C, R_f 0.36 (DCM:MeOH, 9:1).^{1}H NMR (300 MHz, DMSO-d_6) δ 11.14 (s, 1H), 8.97 (s, 1H), 7.83-7.53 (m, 2H), 7.56-7.12 (m, 12H), 4.65 (d, *J* = 9.8 Hz, 1H), 4.34-4.03 (m, 2H), 3.85 (m, 1H), 3.69 (d, *J* = 11.1 Hz,

2H), 3.58 (bs, 1H), 3.18-2.87 (m, 2H), 2.77-2.56 (m, 1H), 1.96-1.78 (m, 1H), 1.76-1.56 (m, 2H). ^{13}C NMR (75 MHz, DMSO-d_6) δ 168.6, 168.0, 164.5, 139.7, 139.6, 139.4, 139.3, 135.7, 131.2, 129.3 (2C), 129.2 (2C), 128.9, 127.9 (2C), 127.3 (2C), 127.1 (2C), 63.8, 61.8, 50.7, 44.4, 30.9, 30.4, 30.1, 29.8. ESI-MS *m/z*: 484 $[M+H]^+$. HRMS (ESI) *m/z* $[M+H]^+$ calculated for $C_{29}H_{30}N_3O_4$ 484.2236 found 484.2239. HPLC Rt (min): 13.11. IR v_{max} 3246, 2927, 2853, 1729, 1622, 1455.

4.4.3. trans-N-(4-(hydroxycarbamoyl)benzyl)-4-(2-oxo-3,4-diphenylazetidin-1-yl)piperidine-1-carboxamide ((±)-**6c**). Following the general procedure for the synthesis of the final compounds, title compound was obtained as a brownish solid, 58% yield, mp 120-122 °C, R_f 0.35 (DCM:MeOH, 9:1). ^{1}H NMR (300 MHz, DMSO-d_6) δ 11.12 (s, 1H), 8.95 (s, 1H), 7.64 (d, J = 8.1 Hz, 2H), 7.51-7.16 (m, 10H), 7.12-6.98 (m, 2H), 4.71 (d, J = 2.0 Hz, 1H), 4.19 (d, J = 5.5 Hz, 2H), 4.11 (s, 1H), 3.87 (dd, J = 33.8, 13.3 Hz, 2H), 3.63-3.44 (m, 1H), 2.71 (dd, J = 25.3, 12.0 Hz, 2H), 1.96-1.55 (m, 4H). ^{13}C NMR (75 MHz, DMSO-d_6) δ 168.1, 164.6, 157.4, 144.8, 139.5, 135.8, 131.4, 129.3, 129.2, 128.9, 127.9, 127.2, 63.9, 61.8, 51.0, 43.7, 42.8, 42.7, 30.5, 30.0. ESI-MS *m/z*: 497 $[M-H]^-$. HRMS (ESI) *m/z* $[M+H]^+$ calculated for $C_{29}H_{31}N_4O_4$ 499.2345 found 499.2328, $[M+Na]^+$ calculated for $C_{29}H_{30}N_4NaO_4$ 521.2165 found 521.2145. HPLC Rt (min): 12.73, 95.7 % purity. IR v_{max} 3228, 2927, 2857, 1739, 1628, 1537 cm^{-1}.

4.4.4. trans-N-hydroxy-3-(4-(4-(2-oxo-3,4-diphenylazetidin-1-yl)piperidine-1-carbonyl)phenyl)propanamide ((±)-**6d**). Following the general procedure for the synthesis of the final compounds, title compound was obtained as a white oil, 62% yield, R_f 0.37 (DCM:MeOH, 9:1). ^{1}H NMR (300 MHz, $CDCl_3$) δ 7.47-7.03 (m, 14H), 4.67 (s, 1H), 4.13 (s, 1H), 3.0-3.52 (m, 3H), 3.12-2.67 (m, 4H), 2.40-2.14 (m, 2H), 2.16-1.41 (m, 6H).^{13}C NMR (75 MHz, $CDCl_3$) δ 170.7, 168.6, 165.4, 142.5, 138.2, 134.8, 133.2, 129.7, 129.2, 129.0, 128.9, 128.6, 127.8, 127.2, 127.0, 126.5, 64.4, 63.2, 51.0, 41.1, 34.0, 31.1, 29.7. ESI-MS *m/z*: 496 $[M-H]^-$. HRMS (ESI) *m/z* $[M+H]^+$ calculated for

$C_{30}H_{32}N_3O_4$ 498.2393 found 498.2404, $[M+Na]^+$ calculated for $C_{30}H_{31}N_3NaO_4$ 520.2212 found 520.2219. HPLC Rt (min): 13.54.

4.4.5. trans-N-hydroxy-4-(3-oxo-3-(4-(2-oxo-3,4-diphenylazetidin-1-yl)piperidin-1-yl)prop-1-en-1-yl)benzamide ((±)-**6e**). Following the general procedure for the synthesis of the final compounds, title compound was obtained as a white oil, 56% yield, R_f 0.35 (DCM:MeOH, 9:1). ^{1}H NMR (300 MHz, CD_3OD) δ 7.70-7.53 (m, 3H), 7.51-7.20 (m, 11H), 4.68 (s, 1H), 4.60-4.35 (m, 1H), 4.15 (s, 1H), 3.80-3.53 (m, 2H), 3.21-2.82 (m, 2H), 2.29-1.73 (m, 4H), 1.70-1.49 (m, 2H). ^{13}C NMR (75 MHz, CD_3OD) δ 170.3, 169.6, 164.4, 138.9, 138.2, 136.4, 136.4, 134.8, 128.8, 128.6, 127.5, 127.4, 127.1, 126.5, 118.7, 63.9, 63.2, 51.0, 40.7, 29.9. ESI-MS *m/z*: 496 $[M+H]^+$. HRMS (ESI) *m/z* $[M+Na]^+$ calculated for $C_{30}H_{29}N_3NaO_4$ 518.2056 found 518.2058. HPLC Rt (min): 13.83.

4.4.6. trans-N-hydroxy-3-(4-(4-(2-oxo-3,4-diphenylazetidin-1-yl)piperidine-1-carbonyl)phenyl)acrylamide ((±)-**6f**). Following the general procedure for the synthesis of the final compounds, title compound was obtained as a white solid, 65% yield, mp 123-124 °C, R_f 0.33. ^{1}H NMR (300 MHz, DMSO-d_6) δ 10.79 (s, 1H), 9.06 (s, 1H), 7.62-7.54 (m, 3H), 7.48-7.27 (m, 11H), 4.73 (s, 1H), 4.40-4.20 (m, 1H), 4.13 (s, 1H), 3.68-3.47 (m, 2H), 3.10-2.79 (m, 4H), 2.08-1.77 (d, J = 21.6 Hz, 2H), 1.45-1.26 (m, 2H). ^{13}C NMR (75 MHz, DMSO-d_6) δ 169.6, 165.9, 165.8, 141.4, 138.2, 134.8, 132.9, 128.8, 128.6, 128.5, 127.7, 127.4, 127.2, 127.0, 126.4, 119.0, 64.0, 63.2, 51.0, 40.8, 30.0. ESI-MS *m/z*: 496 $[M+H]^+$. HRMS (ESI) *m/z* $[M+Na]^+$ calculated for $C_{30}H_{29}N_3NaO_4$ 518.2056 found 518.2061. HPLC Rt (min): 13.74. IR v_{max} 3218, 2928, 2861, 1748, 1629, 1454.

4.4.7. trans-N-hydroxy-4-(3-oxo-3-(4-(2-oxo-3,4-diphenylazetidin-1-yl)piperidin-1-yl)propyl)benzamide ((±)-**6g**). Following the general procedure for the synthesis of the final compounds, title compound was obtained as a white amorphous solid, 45% yield, R_f 0.35. ^{1}H NMR (300 MHz, $CDCl_3$) δ ^{1}H NMR (300 MHz, cd_3od) δ 7.70-7.59 (m, 2H), 7.51-7.19 (m, 12H), 4.64 (d,

J = 1.8 Hz, 1H), 4.36 (dd, *J* = 32.2, 13.1 Hz, 1H), 4.13 (d, *J* = 1.2 Hz, 1H), 3.94-3.75 (m, 1H), 3.64 (s, 1H), 3.09-2.85 (m, 3H), 2.66 (dd, *J* = 15.5, 8.3 Hz, 2H), 1.98 (s, 2H), 1.78 (d, *J* = 11.4 Hz, 2H). ESI-MS *m/z*: 496 $[M-H]^-$. HRMS (ESI) *m/z* $[M+Na]^+$ calculated for $C_{30}H_{31}N_3NaO_4$ 520.2212 found 520.2207. HPLC Rt (min): 13.66.

4.4.8. trans-N-(4-(2-(hydroxyamino)-2-oxoethyl)phenyl)-4-(2-oxo-3,4-diphenylazetidin-1-yl)piperidine-1-carboxamide ((±)-**6h**). Following the general procedure for the synthesis of the final compounds, title compound was obtained as a white solid, 58% yield, mp 122-124 °C, R_f 0.36. ^{1}H NMR (300 MHz, CD_3OD) δ 7.55-6.92 (m, 14H), 4.67 (d, *J* = 2.1 Hz, 1H), 4.15-3.88 (m, 3H), 3.78-3.57 (m, 1H), 3.32 (s, 2H), 2.90 (ddd, *J* = 17.2, 14.1, 7.2 Hz, 2H), 2.08-1.68 (m, 3H), 1.52-1.47 (m, 1H); ^{13}C NMR (75 MHz, CD_3OD) δ 169.6, 169.5, 156.2, 138.4, 138.3, 134.8, 129.5, 128.8, 128.7, 128.6, 128.5, 127.4, 127.1, 126.4, 120.8, 63.9, 63.2, 51.2, 42.8, 42.6, 38.6, 30.0, 29.6. ESI-MS *m/z*: 497 $[M-H]^-$. HRMS (ESI) *m/z* $[M+Na]^+$ calculated for $C_{30}H_{31}N_3NaO_4$ 521.2165 found 521.2165. HPLC Rt (min): 13.40. IR v_{max} 3258, 2927, 1737, 1641, 1517 cm^{-1}.

4.4.9. N-Hydroxy-4-(2-oxo-2-(4-(2-oxo-3,3-diphenylazetidin-1-yl)piperidin-1-yl)ethyl)benzamide (**6i**). Following the general procedure for the synthesis of the final compounds, title compound was obtained as a white solid, 59% yield, mp 136-138 °C, R_f 0.34 (DCM:MeOH, 9:1). ^{1}H NMR (300 MHz, DMSO-d_6) δ 11.23-10.97 (m, 1H), 8.97 (s, 1H), 7.66 (d, *J* = 8.2 Hz, 2H), 7.39-7.09 (m, 12H), 4.24 (d, *J* = 12.4 Hz, 1H), 3.94-3.63 (m, 5H), 3.27 (dd, *J* = 1.1, 0.6 Hz, 1H), 3.17-2.99 (m, 1H), 2.78-2.61 (m, 1H), 1.74 (s, 2H), 1.48 (dd, *J* = 19.9, 11.4 Hz, 2H); ^{13}C NMR (75 MHz, CD_3OD) δ 169.9, 158.3, 144.3, 140.2, 130.6, 128.3, 126.9, 126.9, 126.8, 64.5, 52.3, 49.8, 43.5, 42.3, 29.1. ESI-MS *m/z*: 482 $[M-H]^-$. HRMS (ESI) *m/z* $[M+H]^+$ calculated for $C_{29}H_{30}N_3O_4$ 484.2236 found 484.2234, $[M+Na]^+$ calculated for $C_{29}H_{29}N_3NaO_4$ 506.2056 found 506.2047. HPLC Rt (min): 13.42, 95.73 % purity. IR v_{max} 3224, 2929, 1739, 1626, 1448 cm^{-1}.

4.4.10. N-(4-(Hydroxycarbamoyl)benzyl)-4-(2-oxo-3,3-diphenylazetidin-1-yl)piperidine-1-carboxamide (**6j**). Following the general procedure for the synthesis of the final compounds, title compound was obtained as a brownish solid, 64% yield, mp 142-144 °C, R_f 0.35 (DCM:MeOH, 9:1). ^{1}H NMR (300 MHz, CD_3OD) δ 7.68 (d, *J* = 8.2 Hz, 2H), 7.47-7.13 (m, 12H), 4.38 (s, 2H), 4.03 (d, *J* = 13.6 Hz, 2H), 3.90 (d, *J* = 11.8 Hz, 2H), 3.83 (ddd, *J* = 15.1, 11.0, 4.1 Hz, 1H), 3.03-2.87 (m, 2H), 1.89 (d, *J* = 9.8 Hz, 2H), 1.78-1.60 (m, 2H); ^{13}C NMR (75 MHz, CD_3OD) δ 169.9, 166.6, 158.3, 154.7, 144.4, 140.2, 130.5, 128.3, 127.0, 126.9, 126.8 (2C), 64.4, 52.3, 49.8, 43.6, 42.3, 29.1, 20.1, 13.4. ESI-MS *m/z*: 497 $[M-H]^-$. HRMS (ESI) *m/z* $[M+H]^+$ calculated for $C_{29}H_{31}N_4O_4$ 499.2345 found 499.2329, $[M+Na]^+$ calculated for $C_{29}H_{30}N_4NaO_4$ 521.2165 found 521.2145. HPLC Rt (min): 12.84, 97.65 % purity. IR v_{max} 3228, 2925, 2851, 1732, 1626, 1537 cm^{-1}.

4.4.11. 4-(hydroxycarbamoyl)benzyl 4-(2-oxo-3,3-diphenylazetidin-1-yl)piperidine-1-carboxylate (**6k**). Following the general procedure for the synthesis of the final compounds, title compound was obtained as a yellow oil, 67% yield, R_f 0.37 (DCM:MeOH, 9:1). ^{1}H NMR (300 MHz, Acetone-d_6) δ 10.83 (s, 1H), 9.42 (s, 1H), 7.90-7.75 (m, 2H), 7.58-7.20 (m, 12H), 5.16 (s, 1H), 4.15-4.02 (m, 2H), 3.95 (s, 1H), 3.87-3.70 (m, 1H), 3.05-2.80 (m, 2H), 1.5-1.82 (m, 4H), 1.78-1.60 (m, 2H); ^{13}C NMR (75 MHz, Acetone-d_6) δ 168.2, 154.5, 152.5, 141.2, 140.9, 131.8, 128.5, 128.4, 127.5, 127.0, 127.0, 65.8, 64.6, 52.0, 49.5, 42.4, 29.1. ESI-MS *m/z*: 500 $[M+H]^+$. HRMS (ESI) *m/z* $[M+Na]^+$ calculated for $C_{29}H_{29}N_3NaO_5$ 522.2005 found 522.1995. HPLC Rt (min): 14.60. IR v_{max} 3232, 2926, 1737, 1698 cm^{-1}.

4.4.12. N-(4-(hydroxycarbamoyl)benzyl)-4-(2-oxo-4-(m-tolyl)azetidin-1-yl)piperidine-1-carboxamide ((±)-**6l**). Following the general procedure for the synthesis of the final compounds, title compound was obtained as a white oil, 62% yield, R_f 0.35 (DCM:MeOH, 9:1). ^{1}H NMR (300 MHz, CD_3OD) δ 7.67 (d, *J* = 7.9 Hz, 2H), 7.35-7.12 (m, 6H), 4.69 (dd, *J* = 5.2, 2.2 Hz, 1H), 4.34 (s, 2H), 3.93 (dd, *J* = 33.8, 13.8 Hz, 2H), 3.67-3.49 (m, 1H), 2.89-2.67 (m, 3H), 2.34 (s, 3H), 2.10-1.96 (m,

1H), 1.93-1.82 (m, 1H), 1.78-1.64 (m, 2H), 1.64-1.56 (m, 1H);^{13}C NMR (75 MHz, CD_3OD) δ 168.6, 158.2, 144.4, 139.2, 138.5, 129.0, 128.5, 126.8, 126.7, 126.7, 123.3, 53.2, 51.1, 45.1, 43.4, 42.5, 42.4, 29.9, 29.2, 20.0. ESI-MS *m/z*: 437 $[M+H]^+$. HRMS (ESI) *m/z* $[M+Na]^+$ calculated for $C_{24}H_{28}N_4NaO_4$ 459.2008 found 459.2006. HPLC Rt (min): 10.57.

4.4.13. 4-(2-(3-chlorophenyl)-4-oxoazetidin-1-yl)-N-(4-(hydroxycarbamoyl)benzyl)piperidine-1-carboxamide ((±)-**6m**). Following the general procedure for the synthesis of the final compounds, title compound was obtained as a white solid, 55% yield, mp 182-183 °C, Rf 0.38 (DCM:MeOH, 9:1). ^{1}H NMR (300 MHz, CD_3OD) δ 7.68 (d, *J* = 8.2 Hz, 2H), 7.48-7.41 (m, 1H), 7.40-7.24 (m, 5H), 4.74 (dd, *J* = 5.3, 2.3 Hz, 1H), 4.34 (s, 2H), 3.95 (dd, *J* = 31.5, 13.9 Hz, 2H), 3.66-3.49 (m, 2H), 2.91-2.67 (m, 3H), 1.76-1.66 (m, 2H), 1.41-1.28 (m, 2H); ^{13}C NMR (75 MHz, CD_3OD) δ 168.3, 158.2, 144.4, 141.9, 134.5, 130.5, 130.3, 128.4, 126.8, 126.4, 124.7, 52.5, 51.2, 45.2, 43.5, 42.5, 42.4, 29.9, 29.3. ESI-MS *m/z*: 457 $[M+H]^+$. HRMS (ESI) *m/z* $[M+Na]^+$ calculated for $C_{23}H_{25}ClN_4NaO_4$ 479.1462 found 479.1458. HPLC Rt (min): 10.85. IR v_{max} 3224, 2936, 1733, 1629, 1541 cm^{-1}.

4.5. Human HDAC1/HDAC6 inhibitory assay

OptiPlate-96 black microplates (PerkinElmer) were employed with an assay volume of 60 µL. Human recombinant HDAC1 (BPS Bioscience, Catalog #: 50051) or human recombinant HDAC6 (BPS Bioscience, Catalog #:50006) was diluted in incubation buffer (50 mM Tris−HCl, pH 8.0, 137mM NaCl, 2.7mM KCl, 1 mM $MgCl_2$ and 1 mg/mL bovine serum albumin (BSA)). A total of 52 µL of this dilution was incubated with 3 µL of increasing concentrations of inhibitors in DMSO and 5 µL of fluorogenic substrate ZMAL (Z-(Ac)Lys-AMC)76,77 (126 µM) at 37 °C. After 90 min incubation time, 60 µL of the stock solution (33 µM Trichostatin A and 6 mg/mL trypsin in trypsin buffer [Tris−HCl 50 mM, pH 8.0, NaCl 100 mM]) was added. After the following incubation at 37 °C for 30 min, the fluorescence was measured on a BMG LABTECH POLARstar OPTIMA plate reader

(BMG Labtechnologies, Germany) at an excitation wavelength of 390 nm and an emission wavelength of 460 nm.

4.6. Human HDAC8 inhibitory assay

Recombinant human HDAC8 was purchased as part of the Fluor de Lys HDAC8 fluorometric drug discovery kit (Enzo Life Sciences, No. BMLAK518). Inhibition assays were performed as previously described with minor modifications. The DMSO concentration was kept constant to 0.5%; the enzyme incubated with DMSO only was used as the control. To keep safe from the possibility of slow-binding inhibition, the enzyme was preincubated with the selected compounds 15 min before substrate addition to the mixture. The Fluor de Lys substrate was added at a final concentration of 50 μM, whereas the enzyme was added at a concentration of 0.45U/reaction; the reaction was allowed to proceed for 1 h at 30 °C. TSA (2 μM) within 50 μL of 1× Developer II was added to quench the reaction, and the mixture was further incubated for 1 h at 30 °C. Fluorescence was measured by a plate reader (Varioskan Lux, Thermo Fisher Scientifica) with excitation wavelength at λ = 370 nm and emission wavelength at λ = 450 nm. IC_{50} was estimated by the nonlinear regression curve fit performed by means of GNU/Octave, according to a generalized form of the dose−response curve equation, as reported by Copeland.

4.7. Human HDAC10 inhibitory assay

For the evaluation of their inhibitory activity, different concentrations of the compounds were incubated in a low binding black 96-well plate with 500 ng of human recombinant HDAC10 (BPS Bioscience, San Diego, CA, USA) in an assay buffer composed of 25 mM Tris/HCl, pH 8.0, 137 mM NaCl, 2.7 mM KCl, 1 mM $MgCl_2$, and 0.1 mg/mL bovine serum albumin for 30 min at 37 °C. At the end of the incubation, the deacetylation reaction was initiated by adding 200 μM of a fluorogenic acetylated HDAC substrate (BPS Bioscience). After 30 min at 37 °C, the reaction was stopped by the addiction of an HDAC assay developer (BPS Bioscience). Following incubation of 15 min,

fluorescence was measured in an EnSight multimodal plate reader (Perkin Elmer, Boston, MA, USA) with an excitation wavelength of 360 nm and an emission wavelength of 450 nm.

4.8. Computational details

Molecular docking studies were conducted employing Glide software (Glide, Schrödinger, LLC, New York, NY, release 2016) *via* Maestro Drug Discovery suite release 2015 as previously reported [20,21,60]. Crystal structures of human HDAC1 (PDB ID 4BKX) [61], HDAC6 (PDB ID 5EDU) [62], and HDAC8 (PBD ID 3F0R) [63] were downloaded from PDB and treated by Protein Preparation Wizard (PPW) protocol implemented in Maestro suite for obtaining appropriate protein structures to use in further computational studies. Ligands were built in Maestro suite using available drawing tools. Compounds were minimized using MacroModel software with OPLS-2005 as force field. The resulting molecules were submitted to LigPrep application (LigPrep, Schrödinger, LLC, New York, NY, release 2016) for generating the most probable ionization state at cellular pH (7.4 ± 0.2). Glide calculations were conducted using the scoring function extra precision (XP). Energy grids were prepared using default value of protein atom scaling factor (1.0 Å) within a cubic box centered on the zinc ion which roughly represents the center of the active sites. After grid generation with the introduction of metal constrains, the ligands were docked into the enzymes. The number of poses entered to post-docking minimization was set to 50.

4.9. Cell culture and cell lines

Human colon carcinoma HCT116 (purchased from ATCC, Milano, Italy) were cultured in Dulbecco's Modified Eagle Medium (DMEM; EuroClone, Milano, Italy), supplemented with 10% heat-inactivated fetal bovine serum (FBS; Sigma-Aldrich, St Louis, USA) antimicrobials (100 U/mL penicillin, 100 µg/mL streptomycin, 250 ng/mL amphotericin-B), and 2 mM L-glutamine (EuroClone); , human myeloid leukaemia cell U937 (ATCC) were grown in RPMI 1640 media plus

10% FBS, 100 U/mL penicillin, 100 µg/mL streptomycin, 250 ng/mL amphotericin-B, and 2 mM L-glutamine. The cell lines were routinely checked for mycoplasma contamination.

4.10. Cell viability assay

Cell viability was determined in HCT116 cell line using Thiazolyl Blue Tetrazolium Bromide [(4,5-dimethylthiazol-2-yl)-2,5-diphenyltetrazolium bromide] (MTT; Sigma-Aldrich) assay, following manufacturer's instructions. Cells were seeded in a 48-well plate at a density of 3 x 10^4 cells/well and treated, in triplicate, with compounds at different concentrations (1, 5, 10, and 50 µM) for 24 and 48 h. MTT solution was added at 0.5 mg/mL for 3 h, the purple formazan crystals were dissolved in DMSO and absorbance. Absorbance was read at a wavelength of 570 nm with a TECAN M-200 reader (Tecan, Männedorf, Switzerland). Cell viability was detected in U937 cell line by Cell Counting Kit (CCK-8) assay using WST-8 (2-(2-methoxy-4-nitrophenyl)-3-(4-nitrophenyl)-5-(2,4-disulfophenyl)-2H-tetrazolium, monosodium salt), following manufacturer's protocol. After stimulation with compounds at 1, 5, 10, and 50 µM concentrations for 24 and 48 h in triplicate, 10 µL of CCK-8 solution was added to each well, and the 96-well plate was continuously incubated at 37 °C for 3 h. Then, for each well was read at wavelength 450 nm with a TECAN M-200 reader (Tecan, Männedorf, Switzerland) to determine the cell viability.

4.11. Western blot analysis

After the induction with the tested compounds at 10 µM, HCT116 and U937 cells were harvested and then washed twice with cold 1X PBS and were lysed using a lysis buffer supplemented with protease and phosphatase inhibitors: 50 mM Tris-HCl pH 8.0, 150 mM NaCl, 1% NP40, 10 mM sodium fluoride, 0.1 mM sodium orthovanadate, 40 mg/mL phenylmethylsulfonyl fluoride (PMSF), 20 g/mL aprotinin, 20 mg/mL leupeptin, 2 mg/mL antipain, 10 mM p-nitrophenyl phosphate, 10 mg/ mL pepstatin A and 20 nM okadaic acid. Cells were then centrifuged at 13000 rpm for 30 min at 4 °C, and protein content of supernatant was used to determine the protein concentration by colorimetric

assay (Biorad, Italy). Cell extracts were diluted 1:1 in sample buffer 4X Laemmli (0.217 M Tris-HCl pH 8.0, 52.17% SDS, 17.4% glycerol, 0.026% bromo-phenol blue, 8.7% beta-mercaptoethanol), and then boiled for 3 min. Equal amounts of protein (50 µg) were run and separated by SDS-PAGE gel (acrylamide gel). Primary antibodies used were Acetyl SMC3 (Lys105/106) clone 21A7 (Merck) diluted 1:1000; Acetyl-tubulin and HSP90 acetylated (Sigma) (1:1000); 1:3000 anti-GAPDH antibody (Elabscience) was used for normalization. SAHA (5µM) and PCI (10µM) were used as reference compounds.

4.12. Histone extraction

After the induction with new compounds at 10 µM concentrations and indicated times, HCT116 and U937 cells were harvested and washed twice with cold 1X PBS and lysed in Triton extraction buffer (TEB; PBS containing 0.5% Triton X 100 (v/v), 2 mM PMSF, 0.02% (w/v) NaN3) for 10 min on ice, with gentle stirring. After centrifugation (2000 rpm at 4 °C for 10 min), the supernatant was removed, and the pellet was washed in half the volume of TEB and centrifuged as before. The pellet was overnight incubated in 0.2 N HCl at 4 °C on a rolling table. The samples were then centrifuged at 2000 rpm for 10 min at 4 °C and histone content was determined with Bradford assay (Bio-Rad, CA, USA). For the detection of histone H3 acetylation, H3K9,14ac (Diagenode) was probed on 5µg of histone extracts . Histone H4 (Abcam) antibodies was used to normalize for equal loading.

4.13. RNA isolation and real-time PCR

RNA extraction was performed using TRIzol (Thermo Fisher Scientific) according to supplier's instructions. RNA samples were quantified using NanoDrop 1000 Spectrophotometer V3.8 Thermo Fisher and their quality was checked using an Agilent RNA 6000 Nano kit guide. VILO cDNA Synthesis Kit (Invitrogen, Monza and Brianza, Italy) was used to convert RNA into cDNA. Then, 50 ng of cDNA was used in 1X SYBR Green PCR Master Mix (Bio-Rad), Italy) according to the manufacturer's instructions. Primers used were: HDAC6 (F) TAT CCCCAATCTAGCGGAGG

and (R) CTGCTCATCCAACACCAA GC; HDAC8 (F) GGCTGCGGAACGGTTTTAAG and (R) GCTTCAATCAAAGAATGCACCATAC; Actin (F) CTCCTGAGCGCAAGTACT and (R) CGTCATACTCCTGCTTGC. Analysis was performed by ΔCt and ΔΔCt methods and represents the media of triplicates.

4.13.1. Zebrafish embryos

Zebrafish embryos were raised and maintained under standard condition according to the national guidelines (Italian decree March 4, 2014, n. 26). Embryos from AB strain were collected by natural spawning, staged according to the reference guidelines [64] and raised at 28 °C in E3 medium fish water (instant ocean, 0.1% methylene blue in petri dishes). From the stage of 24 h post-fertilization (hpf) 0.003% 1-phenyl-2-thiourea (PTU, Sigma-Aldrich, Saint Louis, MO) was added to prevent pigmentation. Before manipulations, embryos were dechorionated, and anesthetized with 0.016% tricaine (ethyl 3-aminobenzoate methanesulfonate salt; Sigma-Aldrich).

4.13.2. Western blotting analyses

For zebrafish, at least 40 hpf anesthetized embryos were used for protein extraction after chemical removal of the yolk with deyolking solution to avoid yolk protein contamination. Proteins were collected and prepared using 2 μL/embryo of RIPA buffer (50 mM Tris-HCl pH 7.4, 1% NP-40, 150 mM NaCl, 0.25% sodium deoxycholate, 1 mM EDTA, 1 mM PMSF, protease inhibitors Roche). The lysate concentration was determined according to the manufacturer's instructions of the Quantum Micro BCA protein assay kit (Euroclone, Pero, MI, Italy). Electrophoresis analyses were done by loading 40 μg of proteins onto a 7.5% polyacrylamide gels. After the transfer, PVDF membranes were treated with blocking solution at room temperature for 1 h prior to incubation with the primary antibodies: Vinculin (anti mouse 1:6000, Sigma-Aldrich) and ac-alpha-Tubulin (anti mouse 1:1000; Sigma-Aldrich). After incubation with the HRP-conjugated secondary antibodies for 1h at room temperature (mouse Santa Cruz Biotechnology, Dallas, TX, USA, rabbit Thermofisher, Waltham,

MS, USA), the protein bands were detected using ECL detection systems (Cyangen, Bologna, Italy). Imaging acquisition was performed with the Alliance MINI HD9 AUTO Western Blot Imaging System (UVItec Limited, Cambridge, UK) and analyzed with the related software. Images were processed using the Adobe Photoshop (Microsoft Windows; macOS) software.

4.14.1. Rats

All experimental protocols were approved by the Animal Care and Ethics Committee of the University of Siena and Italian Department of Health (7DF-19.N.TBT) and carried out in accordance with the European Union Guidelines for the Care and the Use of Laboratory Animals (European Union Directive 2010/63/EU). Male Wistar rats (300 g, Charles River Italia, Calco, Italy) were anaesthetized (i.p.) with a mixture of Zoletil® 100 (7.5 mg/kg tiletamine HCl + 7.5 mg/kg zolazepam HCl; Virbac srl, Milano) and Rompun® (8 mg/kg xylazine HCl; Bio 98, San Lazzaro, Bologna), containing heparin (5000 U/kg), decapitated and exsanguinated.

4.13.2. Isolated Rat Heart Preparation and Perfusion

The hearts, spontaneously beating, were rapidly explanted and mounted on a Langendorff apparatus for retrograde perfusion *via* the aorta at a constant flow rate of 10 mL/min with a Krebs−Henseleit solution of the following composition (mM): NaCl 118, KCl 4.7, $CaCl_2$ 2.5, $MgSO_4$ 1.2, $NaHCO_3$ 25, KH_2PO_4 1.2, glucose 11.5, Na pyruvate 2, and EDTA 0.5, bubbled with a 95% O_2−5% CO_2 gas mixture (pH 7.4), and kept at 37 °C, as described elsewhere [65]. Hearts were allowed to equilibrate for at least 20 min before drug exposure. Heart contractility was measured as left ventricle pressure (LVP) by means of latex balloon, inserted into the left ventricle via the mitral valve and connected to a pressure transducer (BLPR, WPI, Berlin, Germany). The balloon was inflated with deionized water from a microsyringe until a left ventricular end diastolic pressure of 10 mmHg was obtained. Alteration in coronary perfusion pressure (CPP), arising from changes in coronary vascular resistance, were recorded by pressure transducer (BLPR, WPI, Berlin, Germany) placed in the inflow

line [66]. A surface electrocardiogram (ECG) was recorded at a sampling rate of 1 kHz by means of two steel electrodes, one placed on the apex and the other on the left atrium of the heart. The ECG analysis included the following measurements: RR (cycle length), HR (frequency), PQ (atrioventricular conduction time), QRS (intraventricular conduction time), and QT (overall action potential duration) [67]. LVP, CPP, and ECG were recorded with a digital PowerLab data acquisition system (PowerLab 8/30; ADInstruments, Castle Hill, Australia) and analyzed by using Chart Pro for Windows software (PowerLab; ADInstruments, Castle Hill, Australia). LVP was calculated by subtracting the left ventricular diastolic pressure from the left ventricular systolic pressure. As the QT interval is affected by heart rate changes (e.g., it shortens when heart rate increases), Bazett's formula normalized to average rat RR (QTc = QT/(RR/ f)1/2) [68] was routinely used to correct it, in order to avoid confounding effects. In our experiments, “f”, the normalization factor according to the basal RR duration was 239.5 ms, as it was the average cardiac cycle length. Analysis of data was accomplished using GraphPad Prism version 5.04 (GraphPad Software, San Diego, USA). Statistical analyses and significance as measured by repeated measures ANOVA (followed by Dunnett’s post test) were obtained using GraphPad InStat version 3.06 (GraphPad Software, San Diego, USA). In all comparisons, $P < 0.05$ was considered significant. Compound **6j** was dissolved in DMSO. Solvent failed to alter the response of the preparations (data not shown).

4.14. HPLC analysis

For the HPLC analysis, a Chromolith HPLC column RP-18 was employed. The runs were performed by gradient elution starting from a mixture 0% MeCN (0.1% TFA as the phase modifier) in H_2O (0.1% TFA as the phase modifier) to 20% MeCN (0.1% TFA) in H_2O (0.1% TFA) in 4 min and then up to 50% MeCN (0.1% TFA) in H_2O in 3 min. The flow speed was set at 0.8 mL/min, and the temperature was maintained at 25 °C. The volume of injection of the sample was 10 µL, and the wavelength selected for the detection was 254 nM.

4.15. Solubility Assay, Chemical Stability at 25 °C and Microsome Stability

A stock solution for each tested compound was prepared by dissolving the sample in DMSO to a final concentration of 10 mM. Three samples were prepared from the stock solution: one used as the standard solution while other two as the test solutions at pH 3.0 and pH 7.4. The concentration of these solutions was 250 μM with a DMSO content of 2.5% (v/v). The standard solution was prepared by dilution of the stock solution in PBS solution (MeCN/water, 60:40), the dilution of the stock solution in 50 mM acetic acid afforded the sample solution at pH 3.0, and the dilution of the stock solution in 50 mM aqueous PBS afforded the sample solution at pH 7.4. These suspensions/solutions were sealed and left for 24 h at 25 °C under orbital shaking to achieve "pseudothermodynamic equilibrium". After that, the solutions were filtered using PTFE filters and successively diluted 1:2 with the buffer solution used for the preparation of the samples. Then, they were analyzed by HPLC/UV/ DAD using UV detection at 254 nm for quantitation. For each sample, the analysis was performed in triplicate, and the solubility result reported was obtained from the average of the three values. The same sample solutions were prepared to evaluate the chemical stability of the compounds after 24 h at 25 °C and analyzed by HPLC/UV/DAD using UV detection at 254 nm for quantitation. Stability was calculated by comparing the area of the peak at T_0 with the area of the peak of the same solution after 24 h, by using this formula:

$$S = \frac{A_{smp}\ x\ FD\ x\ C_{st}}{A_{st}}$$

where S = solubility of the compound (μM); A_{smp} = UV area of the sample solution; FD = dilution factor (2); C_{st} = standard concentration (250 μM) and A_{st} = UV area of the standard solution.

A stability percentage value was calculated by this method at pH 3.0, pH 7.4 and pH 9.2 . Furthermore, the chemical stability has been evaluated at T = 40 °C by heating a methanol solution of the compounds for 24 h overnight or after a 24 h stress under UV = 254 nM. For each sample, the

analysis was performed in triplicate and the stability result reported was obtained from the average of the three values, by using this formula:

$$\% = \frac{AC_{24}}{AC_{T_0}}\ x\ 100$$

where AC_{24} = area of the sample after 24 h at 25 °C; AC_{T0} = area of the sample at T_0.

For the metabolic stability, the tested compound (**6c** or **6j**), dissolved in MeCN, was incubated at 37 °C at 5 μM concentration in 100 mM phosphate buffer (pH 7.4) with 0.5 mg/mL rat, mouse and human liver microsomal proteins. CYP-dependent reactions were started by addition of NADPH-GS (2 mM NADPH), 66 mM glucose-6-phosphate, 0.4 U/ mL glucose-6-phosphate dehydrogenase to 66 mM $MgCl_2$. Reactions were terminated at regular time intervals (overall range 0−60 min) by adding 1 mL of MeCN. All incubations were performed in triplicate. HPLC analysis was performed on a Shimadzu Prominence apparatus equipped with a Chromolith HPLC column RP-18 and coupled with a UV−vis detector, set at λ = 254 nm. The analysis was carried out as described above.[58]

For LogP calculations, we used the same HPLC method used for calculation of solubility and chemical stability, preparing 1mL of a compound stock solution in MeOH (0.005 M). The stock solution has been diluted six times by adding 0.5 mL of MeOH in order to obtain a calibration curve. After that, the compound was partitioned between water and *n*-octanol. LogP was calculated as the ratio between *n*-octanol and water phase of the compound, related to calibration curve.[69]

Acknowledgments

The authors from Department of Biotechnology, Chemistry and Pharmacy acknowledge Ministero dell'Istruzione, Università e della Ricerca (MIUR) for the "Dipartimento di Eccellenza 2018-2022" grant, L. 232/2016. Authors thank prof. Agnese Magnani and prof. Marco Consumi for IR experiments. Authors (GiC, CB, VT and LP) thank Bando Ricerca Salute 2018-Precise-CLL. This

research was funded by VALERE 2019-EPIMS; V:ALERE 2020—“CIRCE”; Campania Regional Government Technology Platform,Lotta alle Patologie Oncologiche iCURE-B21C17000030007; Campania Regional Government FASE2: IDEAL; MIUR, Proof of Concept POC01_00043; MISE: NABUCCO 1682; POR Campania FSE 2014-2020 ASSE III; The author EP was supported by PON RI 2014/2020 “Dottorati Innovativi con caratterizzazione industriale”. Authors (A Pez and AnP) were supported by the Associazione Italiana per la Ricerca sul Cancro (AIRC) (MFAG#18714). The funders had no role in the study design, data collection and interpretation, or the decision to submit the work for publication.

References

[1] M. Fardi, S. Solali, M. Farshdousti Hagh, Epigenetic mechanisms as a new approach in cancer treatment: An updated review, Genes Dis. 5 (2018) 304–311. https://doi.org/https://doi.org/10.1016/j.gendis.2018.06.003.

[2] Y. Li, G. Yang, C. Yang, P. Tang, J. Chen, J. Zhang, J. Liu, L. Ouyang, Targeting Autophagy-Related Epigenetic Regulators for Cancer Drug Discovery, J. Med. Chem. 64 (2021) 11798–11815. https://doi.org/10.1021/acs.jmedchem.1c00579.

[3] M. Cosenza, S. Pozzi, The therapeutic strategy of HDAC6 inhibitors in lymphoproliferative disease, Int. J. Mol. Sci. 19 (2018). https://doi.org/10.3390/ijms19082337.

[4] M. Brindisi, A.P. Saraswati, S. Brogi, S. Gemma, S. Butini, G. Campiani, Old but Gold: Tracking the New Guise of Histone Deacetylase 6 (HDAC6) Enzyme as a Biomarker and Therapeutic Target in Rare Diseases, J. Med. Chem. 63 (2020) 23–39. https://doi.org/10.1021/acs.jmedchem.9b00924.

[5] E. Landucci, M. Brindisi, L. Bianciardi, L.M. Catania, S. Daga, S. Croci, E. Frullanti, C. Fallerini, S. Butini, S. Brogi, S. Furini, R. Melani, A. Molinaro, F.C. Lorenzetti, V. Imperatore, S. Amabile, J. Mariani, F. Mari, F. Ariani, T. Pizzorusso, A.M. Pinto, F.M. Vaccarino, A. Renieri, G. Campiani, I. Meloni, iPSC-derived neurons profiling reveals

GABAergic circuit disruption and acetylated α-tubulin defect which improves after iHDAC6 treatment in Rett syndrome, Exp. Cell Res. 368 (2018) 225–235. https://doi.org/https://doi.org/10.1016/j.yexcr.2018.05.001.

[6] G. Carullo, S. Federico, N. Relitti, S. Gemma, S. Butini, G. Campiani, Retinitis Pigmentosa and Retinal Degenerations: Deciphering Pathways and Targets for Drug Discovery and Development, ACS Chem. Neurosci. 11 (2020) 2173–2191. https://doi.org/10.1021/acschemneuro.0c00358.

[7] G. Campiani, C. Cavella, J.D. Osko, M. Brindisi, N. Relitti, S. Brogi, A.P. Saraswati, S. Federico, G. Chemi, S. Maramai, G. Carullo, B. Jaeger, A. Carleo, R. Benedetti, F. Sarno, S. Lamponi, P. Rottoli, E. Bargagli, C. Bertucci, D. Tedesco, D. Herp, J. Senger, G. Ruberti, F. Saccoccia, S. Saponara, B. Gorelli, M. Valoti, H. Sundaramurthi, S. Butini, M. Jung, K.M. Roach, L. Altucci, P. Bradding, D.W. Christianson, S. Gemma, A. Prasse, Harnessing the Role of HDAC6 in Idiopathic Pulmonary Fibrosis: Design, Synthesis, Structural Analysis, and Biological Evaluation of Potent Inhibitors, (2021).

[8] Y. Hai, D.W. Christianson, Histone deacetylase 6 structure and molecular basis of catalysis and inhibition, Nat. Chem. Biol. 12 (2016) 741–747. https://doi.org/10.1038/nchembio.2134.

[9] T.C.S. Ho, A.H.Y. Chan, A. Ganesan, Thirty Years of HDAC Inhibitors: 2020 Insight and Hindsight, J. Med. Chem. 63 (2020) 12460–12484. https://doi.org/10.1021/acs.jmedchem.0c00830.

[10] S. Banerjee, N. Adhikari, S.A. Amin, T. Jha, Histone deacetylase 8 (HDAC8) and its inhibitors with selectivity to other isoforms: An overview, Eur. J. Med. Chem. 164 (2019) 214–240. https://doi.org/10.1016/j.ejmech.2018.12.039.

[11] A. Chakrabarti, I. Oehme, O. Witt, G. Oliveira, W. Sippl, C. Romier, R.J. Pierce, M. Jung, HDAC8: a multifaceted target for therapeutic interventions, Trends Pharmacol. Sci. 36 (2015) 481–492. https://doi.org/10.1016/j.tips.2015.04.013.

[12] F. Saccoccia, M. Brindisi, R. Gimmelli, N. Relitti, A. Guidi, A.P. Saraswati, C. Cavella, S.

Brogi, G. Chemi, S. Butini, G. Papoff, J. Senger, D. Herp, M. Jung, G. Campiani, S. Gemma, G. Ruberti, Screening and Phenotypical Characterization of Schistosoma mansoni Histone Deacetylase 8 (SmHDAC8) Inhibitors as Multistage Antischistosomal Agents, ACS Infect. Dis. 6 (2020) 100–113. https://doi.org/10.1021/acsinfecdis.9b00224.

[13] M. Duvic, J. Vu, Vorinostat: a new oral histone deacetylase inhibitor approved for cutaneous T-cell lymphoma, Expert Opin. Investig. Drugs. 16 (2007) 1111–1120. https://doi.org/10.1517/13543784.16.7.1111.

[14] C. Grant, F. Rahman, R. Piekarz, C. Peer, R. Frye, R.W. Robey, E.R. Gardner, W.D. Figg, S.E. Bates, Romidepsin: a new therapy for cutaneous T-cell lymphoma and a potential therapy for solid tumors, Expert Rev. Anticancer Ther. 10 (2010) 997–1008. https://doi.org/10.1586/era.10.88.

[15] R.M. Poole, Belinostat: First Global Approval, Drugs. 74 (2014) 1543–1554. https://doi.org/10.1007/s40265-014-0275-8.

[16] X. Lu, Z. Ning, Z. Li, H. Cao, X. Wang, Development of chidamide for peripheral T-cell lymphoma, the first orphan drug approved in China, Intractable Rare Dis. Res. 5 (2016) 185–191. https://doi.org/10.5582/irdr.2016.01024.

[17] M.P. Fenichel, FDA Approves New Agent for Multiple Myeloma, JNCI J. Natl. Cancer Inst. 107 (2015). https://doi.org/10.1093/jnci/djv165.

[18] B.E. Gryder, Q.H. Sodji, A.K. Oyelere, Targeted cancer therapy: giving histone deacetylase inhibitors all they need to succeed, Future Med. Chem. 4 (2012) 505–524. https://doi.org/10.4155/fmc.12.3.

[19] J.E. Amengual, J.K. Lue, H. Ma, R. Lichtenstein, B. Shah, S. Cremers, S. Jones, A. Sawas, First-in-Class Selective HDAC6 Inhibitor (ACY-1215) Has a Highly Favorable Safety Profile in Patients with Relapsed and Refractory Lymphoma, Oncologist. 26 (2021) 184-e366. https://doi.org/10.1002/onco.13673.

[20] A.P. Saraswati, N. Relitti, M. Brindisi, J.D. Osko, G. Chemi, S. Federico, A. Grillo, S. Brogi,

N.H. McCabe, R.C. Turkington, O. Ibrahim, J. O'Sullivan, S. Lamponi, M. Ghanim, V.P. Kelly, D. Zisterer, R. Amet, P. Hannon Barroeta, F. Vanni, C. Ulivieri, D. Herp, F. Sarno, A. Di Costanzo, F. Saccoccia, G. Ruberti, M. Jung, L. Altucci, S. Gemma, S. Butini, D.W. Christianson, G. Campiani, Spiroindoline-Capped Selective HDAC6 Inhibitors: Design, Synthesis, Structural Analysis, and Biological Evaluation, ACS Med. Chem. Lett. 11 (2020) 2268–2276. https://doi.org/10.1021/acsmedchemlett.0c00395.

[21] N. Relitti, A.P. Saraswati, G. Chemi, M. Brindisi, S. Brogi, D. Herp, K. Schmidtkunz, F. Saccoccia, G. Ruberti, C. Ulivieri, F. Vanni, F. Sarno, L. Altucci, S. Lamponi, M. Jung, S. Gemma, S. Butini, G. Campiani, Novel quinolone-based potent and selective HDAC6 inhibitors: Synthesis, molecular modeling studies and biological investigation, Eur. J. Med. Chem. 90 (2020) 112998. https://doi.org/10.1016/j.ejmech.2020.112998.

[22] Y. Depetter, S. Geurs, R. De Vreese, S. Goethals, E. Vandoorn, A. Laevens, J. Steenbrugge, E. Meyer, P. de Tullio, M. Bracke, M. D'hooghe, O. De Wever, Selective pharmacological inhibitors of HDAC6 reveal biochemical activity but functional tolerance in cancer models., Int. J. Cancer. 145 (2019) 735–747. https://doi.org/10.1002/ijc.32169.

[23] S. Balasubramanian, J. Ramos, W. Luo, M. Sirisawad, E. Verner, J.J. Buggy, A novel histone deacetylase 8 (HDAC8)-specific inhibitor PCI-34051 induces apoptosis in T-cell lymphomas, Leukemia. 22 (2008) 1026–1034. https://doi.org/10.1038/leu.2008.9.

[24] Y. Kang, H. Nian, P. Rajendran, W.M. Dashwood, J.T. Pinto, L.A. Boardman, S.N. Thibodeau, P.J. Limburg, C. V. Löhr, W.H. Bisson, D.E. Williams, E. Ho, R.H. Dashwood, HDAC8 and STAT3 repress BMF gene activity in colon cancer cells, Cell Death Dis. 5 (2014) 1–8. https://doi.org/10.1038/cddis.2014.422.

[25] M. Ghiaghi, F. Forouzesh, H. Rahimi, Effect of Sodium Butyrate on LHX1 mRNA Expression as a Transcription Factor of HDAC8 in Human Colorectal Cancer Cell Lines, Avicenna J. Med. Biotechnol. 11 (2019) 317–324.

[26] H. Sundaramurthi, S.L. Roche, G.L. Grice, A. Moran, E.T. Dillion, G. Campiani, J.A.

Nathan, B.N. Kennedy, Selective Histone Deacetylase 6 Inhibitors Restore Cone Photoreceptor Vision or Outer Segment Morphology in Zebrafish and Mouse Models of Retinal Blindness , Front. Cell Dev. Biol. . 8 (2020) 689.

[27] G.R. Vanaja, H.G. Ramulu, A.M. Kalle, Overexpressed HDAC8 in cervical cancer cells shows functional redundancy of tubulin deacetylation with HDAC6, Cell Commun. Signal. 16 (2018) 1–16. https://doi.org/10.1186/s12964-018-0231-4.

[28] A.T. Negmeldin, J.R. Knoff, M.K.H. Pflum, The structural requirements of histone deacetylase inhibitors: C4-modified SAHA analogs display dual HDAC6/HDAC8 selectivity, Eur. J. Med. Chem. 143 (2018) 1790–1806. https://doi.org/10.1016/j.ejmech.2017.10.076.

[29] F.R. Kolbinger, E. Koeneke, J. Ridinger, T. Heimburg, M. Müller, T. Bayer, W. Sippl, M. Jung, N. Gunkel, A.K. Miller, F. Westermann, O. Witt, I. Oehme, The HDAC6/8/10 inhibitor TH34 induces DNA damage-mediated cell death in human high-grade neuroblastoma cell lines, Arch. Toxicol. 92 (2018) 2649–2664. https://doi.org/10.1007/s00204-018-2234-8.

[30] M. Morgen, R.R. Steimbach, M. Géraldy, L. Hellweg, P. Sehr, J. Ridinger, O. Witt, I. Oehme, C.J. Herbst-Gervasoni, J.D. Osko, N.J. Porter, D.W. Christianson, N. Gunkel, A.K. Miller, Design and Synthesis of Dihydroxamic Acids as HDAC6/8/10 Inhibitors, ChemMedChem. 15 (2020) 1163–1174. https://doi.org/10.1002/cmdc.202000149.

[31] D.E. Olson, F.F. Wagner, T. Kaya, J.P. Gale, N. Aidoud, E.L. Davoine, F. Lazzaro, M. Weïwer, Y.-L. Zhang, E.B. Holson, Discovery of the First Histone Deacetylase 6/8 Dual Inhibitors, J. Med. Chem. 56 (2013) 4816–4820. https://doi.org/10.1021/jm400390r.

[32] X. Peng, L. Li, J. Chen, Y. Ren, J. Liu, Z. Yu, H. Cao, J. Chen, Discovery of Novel Histone Deacetylase 6 (HDAC6) Inhibitors with Enhanced Antitumor Immunity of Anti-PD-L1 Immunotherapy in Melanoma, J. Med. Chem. 65 (2022) 2434–2457. https://doi.org/10.1021/acs.jmedchem.1c01863.

[33] S. Guo, S. Yan, W. Li, H. Zhou, J. Yang, Y. Yao, M. Shen, L. Zhang, H.-B. Zhang, L.-C.

Sun, HDAC6 promotes sepsis development by impairing PHB1-mediated mitochondrial respiratory chain function, Aging (Albany. NY). 12 (2020) 5411–5422. https://doi.org/10.18632/aging.102964.

[34] Y. Kang, H. Nian, P. Rajendran, E. Kim, W.M. Dashwood, J.T. Pinto, L.A. Boardman, S.N. Thibodeau, P.J. Limburg, C. V Löhr, W.H. Bisson, D.E. Williams, E. Ho, R.H. Dashwood, HDAC8 and STAT3 repress BMF gene activity in colon cancer cells, Cell Death Dis. 5 (2014) e1476–e1476. https://doi.org/10.1038/cddis.2014.422.

[35] M. Brindisi, S. Maramai, S. Gemma, S. Brogi, A. Grillo, L. Di Cesare Mannelli, E. Gabellieri, S. Lamponi, S. Saponara, B. Gorelli, D. Tedesco, T. Bonfiglio, C. Landry, K.-M. Jung, A. Armirotti, L. Luongo, A. Ligresti, F. Piscitelli, C. Bertucci, M.-P. Dehouck, G. Campiani, S. Maione, C. Ghelardini, A. Pittaluga, D. Piomelli, V. Di Marzo, S. Butini, Development and Pharmacological Characterization of Selective Blockers of 2-Arachidonoyl Glycerol Degradation with Efficacy in Rodent Models of Multiple Sclerosis and Pain, J. Med. Chem. 59 (2016) 2612–2632. https://doi.org/10.1021/acs.jmedchem.5b01812.

[36] P. Sharma, A. Tripathi, P.N. Tripathi, S.K. Prajapati, A. Seth, M.K. Tripathi, P. Srivastava, V. Tiwari, S. Krishnamurthy, S.K. Shrivastava, Design and development of multitarget-directed N-Benzylpiperidine analogs as potential candidates for the treatment of Alzheimer's disease, Eur. J. Med. Chem. 167 (2019) 510–524. https://doi.org/https://doi.org/10.1016/j.ejmech.2019.02.030.

[37] L. Méndez, A. Poeylaut-Palena, E. Mata, Molecular Diversity by Olefin Cross-Metathesis on Solid Support. Generation of Libraries of Biologically Promising β-Lactam Derivatives, Molecules. 23 (2018) 1193. https://doi.org/10.3390/molecules23051193.

[38] M. Zarei, β-Lactam Preparation via Staudinger Reaction with Activated Dimethylsulfoxide, J. Heterocycl. Chem. 54 (2017) 1161–1166. https://doi.org/10.1002/jhet.2685.

[39] S. Aravapalli, H. Lai, T. Teramoto, K.R. Alliston, G.H. Lushington, E.L. Ferguson, R. Padmanabhan, W.C. Groutas, Inhibitors of Dengue virus and West Nile virus proteases based

on the aminobenzamide scaffold, Bioorg. Med. Chem. 20 (2012) 4140–4148. https://doi.org/https://doi.org/10.1016/j.bmc.2012.04.055.

[40] R.I. Storer, A. Pike, N.A. Swain, A.J. Alexandrou, B.M. Bechle, D.C. Blakemore, A.D. Brown, N.A. Castle, M.S. Corbett, N.J. Flanagan, D. Fengas, M.S. Johnson, L.H. Jones, B.E. Marron, C.E. Payne, D. Printzenhoff, D.J. Rawson, C.R. Rose, T. Ryckmans, J. Sun, J.W. Theile, R. Torella, E. Tseng, J.S. Warmus, Highly potent and selective NaV1.7 inhibitors for use as intravenous agents and chemical probes, Bioorg. Med. Chem. Lett. 27 (2017) 4805–4811. https://doi.org/https://doi.org/10.1016/j.bmcl.2017.09.056.

[41] N.A. Larionova, J.M. Ondozabal, X.C. Cambeiro, Reduction of Electron-Deficient Alkenes Enabled by a Photoinduced Hydrogen Atom Transfer, Adv. Synth. \& Catal. 363 (2021) 558–564. https://doi.org/https://doi.org/10.1002/adsc.202000751.

[42] L. Morera, M. Roatsch, M.C.D. Fürst, I. Hoffmann, J. Senger, M. Hau, H. Franz, R. Schüle, M.R. Heinrich, M. Jung, 4-Biphenylalanine- and 3-Phenyltyrosine-Derived Hydroxamic Acids as Inhibitors of the JumonjiC-Domain-Containing Histone Demethylase KDM4A, ChemMedChem. 11 (2016) 2063–2083. https://doi.org/https://doi.org/10.1002/cmdc.201600218.

[43] G. Orlandini, L. Casimiro, M. Bazzoni, B. Cogliati, A. Credi, M. Lucarini, S. Silvi, A. Arduini, A. Secchi, Synthesis and properties of a redox-switchable calix[6]arene-based molecular lasso, Org. Chem. Front. 7 (2020) 648–659. https://doi.org/10.1039/C9QO01379B.

[44] S. Mazzotta, J. Berastegui-Cabrera, G. Carullo, M. Vega-Holm, M. Carretero-Ledesma, L. Mendolia, F. Aiello, F. Iglesias-Guerra, J. Pachón, J.M. Vega-Pérez, J. Sánchez-Céspedes, Serinol-Based Benzoic Acid Esters as New Scaffolds for the Development of Adenovirus Infection Inhibitors: Design, Synthesis, and In Vitro Biological Evaluation, ACS Infect. Dis. 7 (2021) 1433–1444. https://doi.org/10.1021/acsinfecdis.0c00515.

[45] C. Alvarez Ibarra, M. Quiroga, E. Martinez-Santos, E. Toledano, A one pot preparation of

dymethyl n-alkyliminodithiocarbonates, New J. Org. Synth. 23 (2009) 611–616. https://doi.org/10.1080/00304949109457912.

[46] D.J. Hart, D.C. Ha, The Ester Enolate-Imine Condensation Route to β-Lactams, Chem. Rev. 89 (1989) 1447–1465. https://doi.org/10.1021/cr00097a003.

[47] T. Mandal, S. Jana, J. Dash, Zinc-Mediated Efficient and Selective Reduction of Carbonyl Compounds, European J. Org. Chem. 2017 (2017) 4972–4983. https://doi.org/https://doi.org/10.1002/ejoc.201700887.

[48] D. Zhao, B. Sun, J. Ren, F. Li, S. Song, X. Lv, C. Hao, M. Cheng, Synthesis and biological evaluation of 3-phenyl-3-aryl carboxamido propanoic acid derivatives as small molecule inhibitors of retinoic acid 4-hydroxylase (CYP26A1), Bioorg. Med. Chem. 23 (2015) 1356–1365. https://doi.org/https://doi.org/10.1016/j.bmc.2014.11.036.

[49] Y. Zhu, G. Wu, X. Zhu, Y. Ma, X. Zhao, Y. Li, Y. Yuan, J. Yang, S. Yu, F. Shao, M. Lei, Synthesis, in Vitro and in Vivo Biological Evaluation, and Comprehensive Understanding of Structure−Activity Relationships of Dipeptidyl Boronic Acid Proteasome Inhibitors Constructed from β-Amino Acids, J. Med. Chem. 53 (2010) 8619–8626. https://doi.org/10.1021/jm1009742.

[50] M. Brindisi, J. Senger, C. Cavella, A. Grillo, G. Chemi, S. Gemma, D.M. Cucinella, S. Lamponi, F. Sarno, C. Iside, A. Nebbioso, E. Novellino, T.B. Shaik, C. Romier, D. Herp, M. Jung, S. Butini, G. Campiani, L. Altucci, S. Brogi, Novel spiroindoline HDAC inhibitors: Synthesis, molecular modelling and biological studies, Eur. J. Med. Chem. 157 (2018) 127–138. https://doi.org/https://doi.org/10.1016/j.ejmech.2018.07.069.

[51] J. Melesina, C. V. Simoben, L. Praetorius, E.F. Bülbül, D. Robaa, W. Sippl, Strategies To Design Selective Histone Deacetylase Inhibitors, ChemMedChem. 16 (2021) 1336–1359. https://doi.org/10.1002/cmdc.202000934.

[52] S. Balasubramanian, J. Ramos, W. Luo, M. Sirisawad, E. Verner, J.J. Buggy, A novel histone deacetylase 8 (HDAC8)-specific inhibitor PCI-34051 induces apoptosis in T-cell

lymphomas., Leukemia. 22 (2008) 1026–34. https://doi.org/10.1038/leu.2008.9.

[53] T. Gligoris, J. Löwe, Structural Insights into Ring Formation of Cohesin and Related Smc Complexes., Trends Cell Biol. 26 (2016) 680–693. https://doi.org/10.1016/j.tcb.2016.04.002.

[54] J.-M. Peters, A. Tedeschi, J. Schmitz, The cohesin complex and its roles in chromosome biology., Genes Dev. 22 (2008) 3089–114. https://doi.org/10.1101/gad.1724308.

[55] T. Dasgupta, J. Antony, A.W. Braithwaite, J.A. Horsfield, HDAC8 Inhibition Blocks SMC3 Deacetylation and Delays Cell Cycle Progression without Affecting Cohesin-dependent Transcription in MCF7 Cancer Cells., J. Biol. Chem. 291 (2016) 12761–12770. https://doi.org/10.1074/jbc.M115.704627.

[56] M. Van Damme, E. Crompot, N. Meuleman, P. Mineur, D. Bron, L. Lagneaux, B. Stamatopoulos, HDAC isoenzyme expression is deregulated in chronic lymphocytic leukemia B-cells and has a complex prognostic significance, Epigenetics. 7 (2012) 1403–1412. https://doi.org/10.4161/epi.22674.

[57] M. Spreafico, M. Cafora, C. Bragato, D. Capitanio, F. Marasca, B. Bodega, C. De Palma, M. Mora, C. Gelfi, A. Marozzi, A. Pistocchi, Targeting HDAC8 to ameliorate skeletal muscle differentiation in Duchenne muscular dystrophy., Pharmacol. Res. 170 (2021) 105750. https://doi.org/10.1016/j.phrs.2021.105750.

[58] G. Campiani, C. Cavella, J.D. Osko, M. Brindisi, N. Relitti, S. Brogi, A.P. Saraswati, S. Federico, G. Chemi, S. Maramai, G. Carullo, B. Jaeger, A. Carleo, R. Benedetti, F. Sarno, S. Lamponi, P. Rottoli, E. Bargagli, C. Bertucci, D. Tedesco, D. Herp, J. Senger, G. Ruberti, F. Saccoccia, S. Saponara, B. Gorelli, M. Valoti, B. Kennedy, H. Sundaramurthi, S. Butini, M. Jung, K.M. Roach, L. Altucci, P. Bradding, D.W. Christianson, S. Gemma, A. Prasse, Harnessing the Role of HDAC6 in Idiopathic Pulmonary Fibrosis: Design, Synthesis, Structural Analysis, and Biological Evaluation of Potent Inhibitors, J. Med. Chem. 64 (2021) 9960–9988. https://doi.org/10.1021/acs.jmedchem.1c00184.

[59] G. Sirasani, L. Tong, E.P. Balskus, A Biocompatible Alkene Hydrogenation Merges Organic

Synthesis with Microbial Metabolism, Angew. Chemie Int. Ed. 53 (2014) 7785–7788. https://doi.org/https://doi.org/10.1002/anie.201403148.

[60] M. Brindisi, J. Senger, C. Cavella, A. Grillo, G. Chemi, S. Gemma, D.M. Cucinella, S. Lamponi, F. Sarno, C. Iside, A. Nebbioso, E. Novellino, T.B. Shaik, C. Romier, D. Herp, M. Jung, S. Butini, G. Campiani, L. Altucci, S. Brogi, Novel spiroindoline HDAC inhibitors: Synthesis, molecular modelling and biological studies, Eur. J. Med. Chem. 157 (2018) 127–138. https://doi.org/10.1016/j.ejmech.2018.07.069.

[61] C.J. Millard, P.J. Watson, I. Celardo, Y. Gordiyenko, S.M. Cowley, C. V. Robinson, L. Fairall, J.W.R. Schwabe, Class I HDACs Share a Common Mechanism of Regulation by Inositol Phosphates, Mol. Cell. 51 (2013) 57–67. https://doi.org/10.1016/j.molcel.2013.05.020.

[62] Y. Hai, D.W. Christianson, Histone deacetylase 6 structure and molecular basis of catalysis and inhibition, Nat. Chem. Biol. 12 (2016) 741–747. https://doi.org/10.1038/nchembio.2134.

[63] D.P. Dowling, S.L. Gantt, S.G. Gattis, C.A. Fierke, D.W. Christianson, Structural Studies of Human Histone Deacetylase 8 and Its Site-Specific Variants Complexed with Substrate and Inhibitors , Biochemistry. 47 (2008) 13554–13563. https://doi.org/10.1021/bi801610c.

[64] C.B. Kimmel, W.W. Ballard, S.R. Kimmel, B. Ullmann, T.F. Schilling, Stages of embryonic development of the zebrafish., Dev. Dyn. 203 (1995) 253–310. https://doi.org/10.1002/aja.1002030302.

[65] S. Saponara, M. Kawase, A. Shah, N. Motohashi, J. Molnar, K. Ugocsai, G. Sgaragli, F. Fusi, 3,5-Dibenzoyl-4-(3-phenoxyphenyl)-1,4-dihydro-2,6-dimethylpyridine (DP7) as a new multidrug resistance reverting agent devoid of effects on vascular smooth muscle contractility, Br. J. Pharmacol. 141 (2004) 415–422. https://doi.org/https://doi.org/10.1038/sj.bjp.0705635.

[66] A. Ferrara, F. Fusi, B. Gorelli, G. Sgaragli, S. Saponara, Effects of freeze-dried red wine on cardiac function and ECG of the Langendorff-perfused rat heart, Can. J. Physiol. Pharmacol.

92 (2014) 171–174. https://doi.org/10.1139/cjpp-2013-0262.

[67] F. Pessina, A. Gamberucci, J. Chen, B. Liu, P. Vangheluwe, B. Gorelli, S. Lorenzini, O. Spiga, A. Trezza, G. Sgaragli, S. Saponara, Negative chronotropism, positive inotropism and lusitropism of 3,5-di-t-butyl-4-hydroxyanisole (DTBHA) on rat heart preparations occur through reduction of RyR2 Ca2+ leak, Biochem. Pharmacol. 155 (2018) 434–443. https://doi.org/https://doi.org/10.1016/j.bcp.2018.07.026.

[68] J. Kmecova, J. Klimas, Heart rate correction of the QT duration in rats, Eur. J. Pharmacol. 641 (2010) 187–192. https://doi.org/https://doi.org/10.1016/j.ejphar.2010.05.038.

[69] J.A. Rothwell, A.J. Day, M.R.A. Morgan, Experimental determination of octanol-water partition coefficients of quercetin and related flavonoids., J. Agric. Food Chem. 53 (2005) 4355–60. https://doi.org/10.1021/jf0483669.